This is the accepted manuscript version of the contribution published as:

Lettau, E., **Till, J.**, **Toepel, J.**, Appel, J., Boehm, M., **Sacco, D.**, Lorent, C., Teutloff, C., Mach, R.L., Gutekunst, K., **Bühler, B.**, Lauterbach, L. (2025): Engineering O_2-tolerant chimeric hydrogenases optimized for ferredoxin coupling in *Synechocystis* sp. PCC 6803 *ACS Synth. Biol.* **14** (11), 4478 - 4495

The publisher's version is available at:

https://doi.org/10.1021/acssynbio.5c00494

Engineering O_2-tolerant chimeric hydrogenases optimized for ferredoxin coupling in *Synechocystis* sp. PCC 6803

Elisabeth Lettau‡ [a,b], Jacky Till‡ [c,d], Jörg Toepel [c], Jens Appel [e], Marko Boehm [e], Diletta Sacco [c], Christian Lorent [b], Christian Teutloff [f], Robert L. Mach[d], Kirstin Gutekunst [e], Bruno Bühler [c] and Lars Lauterbach* [a,g]

‡ contributed equally to this work

*Corresponding author: lars.lauterbach@iamb.rwth.aachen.de (Lars Lauterbach)

[a] RWTH Aachen University, iAMB – Institute of Applied Microbiology, Worringerweg 1, 52074 Aachen (Germany)
[b] Technische Universität Berlin, Institute for Chemistry, Straße des 17. Juni 135, 10623 Berlin (Germany)
[c] Helmholtz Centre for Environmental Research – UFZ-Leipzig, Department of Microbial Biotechnology, Permoserstraße 15, 04318 Leipzig, (Germany)
[d] TU Wien, Institute of Chemical, Environmental and Bioscience Engineering – ICEBE, Gumpendorfer Straße 1a, 1060 Wien (Austria)
[e] Universität Kassel, Institut für Biologie, Heinrich-Plett-Straße 40, 34132 Kassel (Germany)
[f] Freie Universität Berlin, Institute für Physik, Arnimallee 14, 14195 Berlin (Germany)
[g] Fraunhofer-Institut für Molekularbiologie und Angewandte Ökologie IME, Forckenbeckstr. 6, 52074 Aachen (Germany)

Keywords: Hydrogenases, protein design, chimeric enzymes, H_2 production, *Synechocystis* sp. PCC 6803, *Cupriavidus necator* H16

Abstract. The development of hydrogenases capable of operating under oxygenic photosynthetic conditions remains a key challenge for sustainable biohydrogen production. In this study, we developed a series of chimeric NAD^+-reducing [NiFe]-hydrogenases (SH) combining structural elements from the O_2-tolerant SH of *Cupriavidus necator* (*Cn*SH) and the ferredoxin-interacting SH of *Synechocystis* sp. PCC6803 (*Syn*SH). By engineering chimeric HoxU and HoxF subunits, we developed constructs—MixSH, Ch-HoxEF$_{Syn}$+U$_{Cn}$, and Ch-HoxU^{swapCTD}—that successfully couple the *Cn*HoxYH hydrogenase module to the *Syn*HoxEFU reductase module while retaining O_2 tolerance and enhancing interaction with reduced ferredoxin. The lithoautotrophic growth of *C. necator* confirmed the tolerance of these variants to O_2, while activity assays in *Synechocystis* demonstrated partial hydrogenase function, including H_2 consumption and fermentative H_2 production. Notably, Ch-HoxEF$_{Syn}$+U$_{Cn}$ retained ferredoxin interaction despite lacking the [4Fe4S]^{U4} cluster, showing [2Fe2S]^{F2} in HoxF as a functional ferredoxin-binding site. Moreover, we achieved the artificial integration of a [2Fe2S] cluster into *Cn*HoxF and identified the *Cn*HoxF N-terminal domain as structurally and functionally analogous to *Syn*HoxE. Although electron transfer efficiency and activity in *Synechocystis* remained limited, this work validates the modular engineering of [NiFe]-hydrogenases, uniting O_2-tolerance with ferredoxin interaction and offering a foundational step towards photosynthesis-coupled H_2 production.

Introduction

The quest for sustainable energy has led to significant research on the use of photosynthetic microorganisms for hydrogen (H_2) production. Among the promising methods, dark fermentation and photosynthetic pathways have attracted attention, with the latter offering the potential for direct photosynthesis-driven H_2 production.[1] Hydrogenases are enzymes capable of converting protons to molecular hydrogen, relying on electrons that can be supplied, for example, by the photosynthetic electron transport chain (PET).[2] The classical electron acceptors reduced during photosynthesis are the ferredoxin 1 (PetF) and subsequently the cofactor NADPH, mediated by the ferredoxin-$NADP^+$-reductase (FNR).[3] From these, ferredoxin (E'^0 = -430mV) is favored for H_2 (E'^0 = -413mV) production due to its lower redox potential compared to NADPH (E'^0 = -320mV). However, challenges such as the oxygen sensitivity of hydrogenases,[4–6] competition from alternative electron pathways such as FNR and the Calvin-Benson-Bassham (CBB) cycle,[3,7,8] and inappropriate cofactor interactions have limited their efficiency.[9] To overcome these obstacles, the development of engineered chimeric hydrogenases represents a novel approach that offers improved catalytic efficiency and stability by combining features from different natural enzymes. Researchers have addressed this by creating fusion proteins of PetF with [FeFe] hydrogenase HydA from *Chlamydomonas reinhardtii* (Fd-Hyd), resulting in enhanced photosynthesis-coupled H_2 production.[10,11] An alternative strategy addressed the fusion of hydrogenases directly to PS I, bypassing ferredoxin as an intermediate. This approach has led to the design of chimeras with PS I such as with the membrane-bound [NiFe] hydrogenase (MBH) from *Cupriavidus necator* H16,[12,13] the hydrogenase module (HoxYH) from the cyanobacterial [NiFe] hydrogenase from *Synechocystis* sp. PCC 6803,[14] and the [FeFe] hydrogenase HydA2 from *Ch. reinhardtii*.[15] These chimeras have demonstrated sustained H_2 production, a critical factor for industrial applications. However, these efforts have primarily addressed cofactor competition and have faced challenges related to O_2 sensitivity, inefficient electron transfer due to large distances between iron-sulfur clusters or have only been applicable for *in vitro* use. Overcoming these limitations requires the design of chimeric hydrogenases that integrate the desired properties of both O_2 tolerance and effective interaction with suitable electron carriers, such as ferredoxin: properties of NAD^+-reducing hydrogenases (SH) from *C. necator* and *Synechocystis*, respectively.[1,16,17]

The SHs of bacteria consist of a hydrogenase module (HoxYH) with a [NiFe] active site responsible for H_2 conversion and a reductase module (HoxFU, previous name diaphorase module), that transfers electrons to redox partners such as $NAD(P)^+$/H (Figure 1 A).[18,19] While some reductase modules of bacterial SHs are supplemented by two further subunits HoxI$_2$,[20–22] the cyanobacterial SHs consist of a non-related additional subunit HoxE in the reductase module (Figure 1 B).[23]

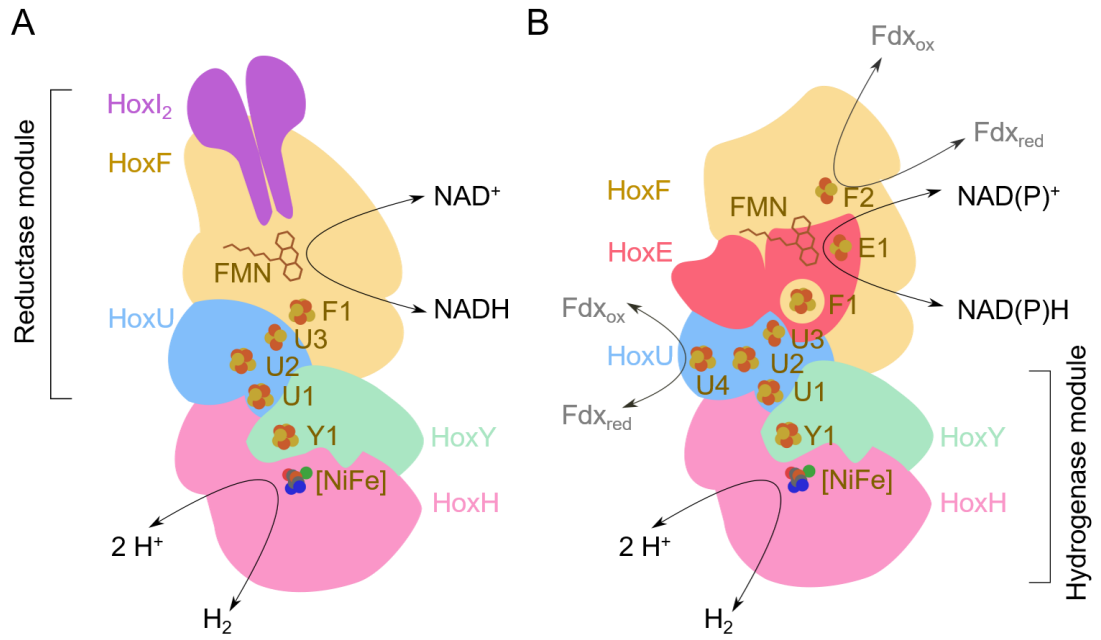


Figure 1) Composition and comparison of NAD⁺ reducing hydrogenases. The subunit composition of the reductase module differs between the two hydrogenases. While the bacterial SH from *C. necator* (A) contains two HoxI subunits, the cyanobacterial SH from *Synechocystis* (B) contains the non-homologous subunit HoxE. In addition, the cyanobacterial SHs have binding motifs for three additional iron-sulfur clusters in HoxF, HoxE and HoxU (here: F2, E1 and U4).

The SH from *C. necator* (*Cn*SH) provides O_2 tolerance by detoxifying it to converting it to H_2O and H_2O_2 at the [NiFe] active site.[17] However, wild-type *Cn*SH is unable to interact with photosynthesis-related electron acceptors NADPH or ferredoxin. Engineered variants of *C. necator* hydrogenase have shown low catalytic efficiencies for $NADP^+$-reduction, nevertheless NADPH-dependent H_2 production has not been demonstrated.[24] In contrast, *Synechocystis* hydrogenase (*Syn*SH) has been shown to produce H_2 from NADH, NADPH, reduced flavodoxin and ferredoxin.[1] The HoxF subunit of *Syn*SH is responsible for NAD(P)H binding, while the HoxE subunit, which contains an additional $[2Fe2S]^{E1}$ binding site, was previously proposed to interact with ferredoxin.[25] However, recent docking studies suggest that electrons from ferredoxin are more likely to be received via an additional $[2Fe2S]^{F2}$ cluster in HoxF or a $[4Fe4S]^{U4}$ cluster in HoxU.[9] In addition, the HoxE subunit, which is critical for the functionality of *Syn*SH,[9,23,26] could play a key role in the design of O_2-tolerant, ferredoxin-interacting chimeric hydrogenases. Therefore, the design strategy may involve either integrating the missing iron-sulfur clusters into the *Cn*SH or coupling the complete *Synechocystis* reductase module (*Syn*HoxEFU) to the *C. necator* hydrogenase module (*Cn*HoxYH).

Rational protein design was chosen over gene shuffling in this study since the HoxF and HoxU subunits of *Cn*SH and *Syn*SH share only 36.12% and 36.16% identity, respectively, well below the threshold for effective gene shuffling. Gene shuffling is typically more successful with enzymes that have more than 70% sequence identity and simpler structures.[27] In addition, *C. necator* was chosen as the host organism for the protein design because it is a well-established platform for the heterologous production of various SHs.[9,28,29] This makes it an ideal platform for expressing and testing the engineered chimeric variants. Photosynthesis-driven H_2 production by the chimeric variants was finally analyzed in the photosynthetic active cyanobacterium *Synechocystis*, which has recently been established as a heterologous host for the native *Cn*SH and thus was supposed to allow expression of chimeric hydrogenases.[30]

Additionally, enhanced activity of *Cn*SH in *Synechocystis* was achieved with addition of the native maturation system of *C. necator*.[31]
The chimeric hydrogenase variants described here, which integrate the strengths of both enzymes, form a promising basis for efficient, photosynthesis-driven H_2 production. By overcoming challenges such as O_2 sensitivity, cofactor interaction and electron transfer efficiency, these engineered enzymes have the potential to revolutionize sustainable H_2 production and offer a promising solution to the global energy crisis.

2. Results and Discussion

2.1. Structural predictions enable targeted design of chimeric hydrogenases. For the successful rational design of chimeric hydrogenases, information on the structure of wild-type hydrogenases is essential. Although the structures of *Cn*SH and *Syn*SH have not yet been solved, spectroscopic methods have provided information on the cofactor composition of both hydrogenases.[9,25,32–35] In addition, homology models could provide at least superficial structural information.[25] However, structure prediction and calculation techniques have become much more accurate and reliable in recent years, providing an alternative basis for rational design of chimeric hydrogenases despite the lack of protein structures. The protein structures for both enzymes, *Cn*SH and *Syn*SH, were calculated using AlphaFold 3.0 and the corresponding cofactors were integrated using AlphaFill (Figure S1 A/B).[36–39] The structural calculations for both *Cn*SH and *Syn*SH showed high confidence, with an overall per-atom confidence (pIDDT) above 90. Slightly lower confidence scores (pIDDT 70-90) were observed for the HoxI subunits of *Cn*SH and the N-terminal domain (NTD) of *Syn*HoxF (Figure S1). The accuracy of the overall structures, as assessed by the predicted template modelling score (pTM), was 0.82 for *Cn*SH and 0.85 for *Syn*SH, indicating strong agreement with the true structures. Furthermore, the predicted relative positioning of the subunits within the complexes, assessed by the interface predicted modelling score (ipTM),[40,41] yielded values of 0.84 and 0.87, respectively, confirming the high quality of the structural predictions.
These structures provide new insights into the subunit composition and organization of the domains associated with ferredoxin interaction. Probably due to gene duplication, the cyanobacterial subunit HoxE shares homology with the NTD of HoxF.[42] In *Synechocystis*, both HoxE and the HoxF NTD contain binding motifs for the [2Fe2S] cluster, whereas only two of the coordinating cysteines are conserved in *Cn*HoxF (Figure S2 A). However, the *Cn*HoxF NTD is 49 amino acids (aa) longer than that of *Syn*HoxF, and the organization of these domains is markedly different in the two hydrogenases. In *Cn*SH, the HoxF NTD is positioned similarly to HoxE in *Syn*SH, sitting laterally next to the FMN binding site. In contrast, the *Syn*HoxF NTD is bent outwards and lies posterior to the HoxE subunit (Figure S2 B/C).
A comparison of the two HoxF subunits also reveals a notable difference in the C-terminal domain (CTD) of *Cn*HoxF, which is extended by 30 amino acids (Figure S3 A). The extended CTD forms a helix that bridges to the hydrogenase module, creating a strong contact with it. A similar feature is observed in the SH of *Hydrogenophilus thermoluteolus* (*Ht*SH): The C-terminal helix interacts with the reductase module when the enzyme is in its oxidized state but bridges to the hydrogenase module when the enzyme is reduced using the artificial reductant dithionite/methyl viologen (Figure S3 B). Additional differences between *Cn*SH and *Syn*SH are evident in the interface regions between the reductase module subunit HoxU and the hydrogenase module subunit HoxY (Figure S4 A/B). These interface regions consist of two loops: 118MV/121DH and 207RVGYDDPIGR/211GETTAE. In *Cn*SH, the second interface region contains a larger number of amino acids involved in hydrophilic-hydrophobic interactions. In addition, the *Cn*HoxU-HoxY interface region contains a significantly higher proportion of hydrophobic amino acids (41.7% compared to 12.5% in *Syn*HoxU, Table S1),

which promotes inter-subunit connections. These findings provide several possibilities for the rational design of chimeric hydrogenases, and a number of chimeras have been developed in which one or more of the above-mentioned domains of the *Synechocystis* and *C. necator* reductase modules have been replaced by the homologous domains of the other (Figure 2).

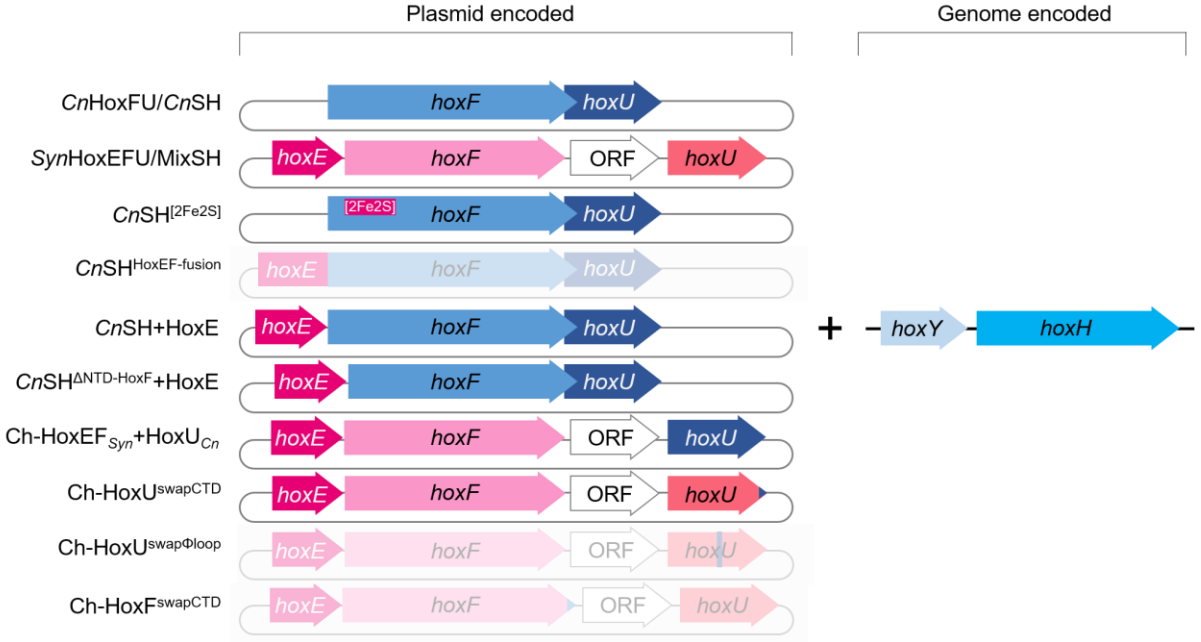


Figure 2) Construction of the chimeric hydrogenases for production in *C. necator* HF903. Parts originating from *C. necator* are shown in blue colors and those from *Synechocystis* in red colors. To simplify genetic construction, the reductase modules were encoded on plasmids and the *C. necator* hydrogenase module was genome-encoded to reduce plasmid size. ORF – open reading frame derived from the natural *hox* operon of *Synechocystis*. Variants shown in fader colors were excluded from further investigation as the study progressed.

2.2. Integration of an additional iron-sulfur cluster from SynSH into CnSH. The incorporation of metallocentres into protein scaffolds has previously been described for proteins without any metallocentres or as part of de novo protein design.[43,44] The integration of iron-sulfur clusters into multimeric and multi-cofactor containing proteins, however, is a novel approach. Since two of the four cysteines required for coordinating a $[2Fe2S]^{F2}$ cluster are already present in the *Cn*HoxF NTD, we substituted the remaining two amino acids, along with their surrounding homologous amino acids, with those from *Syn*HoxE. This resulted in the variant $CnSH^{HoxF\text{-}IA79AC/LSDQE119ACGIA}$ (resp. $CnSH^{[2Fe2S]}$) (Figure S2 A). After a one-step gravity-flow affinity purification, four subunits HoxFUYH of a functional *Cn*SH can be identified on an SDS-PAGE (Figure S5 A). To verify the successful integration of the iron-sulfur cluster into *Cn*HoxF, the wild-type *Cn*SH and its $CnSH^{[2Fe2S]}$ variant were reduced with a 50-fold excess of sodium dithionite (DT) and analyzed by electron paramagnetic resonance (EPR) spectroscopy. At 35K, *Cn*SH exhibits a pronounced rhombic signal related to the [2Fe2S] cluster in HoxU (g_x = 2.048, g_y = 1.958, g_z = 1.931), alongside a weak isotropic species related to the semiquinone radical form of FMN, as previously observed.[45] In contrast, the spectrum of $CnSH^{[2Fe2S]}$ clearly shows an additional rhombic signal (g_x = 2.005, g_y = 1.937, g_z = 1.915) (Figure S5 B). This spectroscopic signature is similar to that of $[2Fe2S]^{F2}$ and $[2Fe2S]^{E1}$ in *Syn*HoxEFU as well as the homologue cluster in respiratory complex I (RC I).[9,25,33,46] In addition, the power saturation is almost identical to that of $[2Fe2S]^{E1}$ in *Syn*HoxE and *Syn*HoxEFU,[9] suggesting the absence of any detectable magnetic coupling to other paramagnetic centers in the vicinity (Table S2).

Together, these data confirm the successful incorporation of a [2Fe2S]^{F2} into the HoxF subunit of *Cn*SH.

The isolated *Cn*SH$^{[2Fe2S]}$ was biochemically characterized by photometric measurements of H_2-dependent NAD^+ reduction. This resulted in a specific activity of 124.2 U mg^{-1}, which is comparable to that of the wild-type *Cn*SH (Table S3).[47] H_2 production rates, as determined by gas chromatography, also showed no significant difference between the wild-type and its variant. When sodium dithionite (DT) was used as the electron donor, a proton reduction activity of 0.031 ± 0.006 U mg^{-1} was observed for *Cn*SH$^{[2Fe2S]}$.

However, structural models of *Cn*SH and *Syn*SH, together with previous docking studies with ferredoxin, indicate that both [2Fe2S] clusters of *Syn*HoxEF (E1 and F2) are essential for electron transfer from ferredoxin.[9,25] This suggests that the integration of a third iron-sulfur cluster into *Cn*HoxF may be required for effective ferredoxin interaction. Unfortunately, the protein sequence of *Cn*HoxF does not provide any further possibility to reactivate an originally existing iron-sulfur cluster. To create an additional coordination site for a [2Fe2S], the *SynhoxE* gene was integrated into the *C. necator* reductase module operon, resulting in chimeras *Cn*SH$^{HoxEF\text{-}fusion}$, *Cn*SH$^{\Delta NTD\text{-}HoxF}$+HoxE and *Cn*SH+HoxE. While *Cn*SH$^{HoxEF\text{-}fusion}$ is a fusion protein of *Syn*HoxE and *Cn*HoxF, HoxE is coproduced to the subunits of *Cn*SH in chimeras *Cn*SH$^{\Delta NTD\text{-}HoxF}$+HoxE and *Cn*SH+HoxE. Although the fusion of *Syn*HoxE and *Cn*HoxF in *Cn*SH$^{HoxEF\text{-}fusion}$ resulted in a stable enzyme with activities and properties comparable to wild-type *Cn*SH (Figure S6 A-E), EPR spectroscopic measurements revealed that the integration of [2Fe2S]^{E1} was not successful (Figure S7 A). This is likely due to insufficient incorporation during maturation, as an AlphaFold model of *Cn*SH$^{HoxEF\text{-}fusion}$ (Figure S7 B) suggests unnatural protein folding, as detailed in Supplementary Information I. Consequently, *Cn*SH$^{HoxEF\text{-}fusion}$ was excluded from further investigation in *C. necator*.

The co-production of *Syn*HoxE and *Cn*SH in the *Cn*SH+HoxE chimera resulted in an enzyme that could be isolated in good yield (6.6 mg protein per 10 g cell pellet) and high purity. However, *Syn*HoxE either dissociated during purification or failed to integrate into the protein complex (Figure S8). As discussed above, our structural models suggest that the HoxF NTD in *Cn*SH occupies a position identical to that of HoxE in *Syn*SH (Figure S2 B/C), likely preventing *Syn*HoxE from being incorporated into the complex. To address this, the *Cn*HoxF NTD in *Cn*SH$^{\Delta NTD\text{-}HoxF}$+HoxE was shortened to match the length of the *Syn*HoxF NTD, thus creating space for *Syn*HoxE integration. Although a faint band corresponding to HoxE was observed in the SDS gel, *Cn*SH$^{\Delta NTD\text{-}HoxF}$+HoxE was only isolated in small amounts and non-specific bands indicative of unstable SH derivatives were also observed (Figure S8).[48] This suggests that *Syn*HoxE incorporation may be possible, making *Cn*SH$^{\Delta NTD\text{-}HoxF}$+HoxE a potential candidate for combination with the *Cn*SH$^{[2Fe2S]}$ substitutions. However, due to the instability of *Cn*SH$^{\Delta NTD\text{-}HoxF}$+HoxE and the limited quantities obtained, this approach was ultimately abandoned.

The integration of a [2Fe2S] cluster into *C. necator* SH through both direct amino acid substitutions and combination with the *Synechocystis* HoxE subunit shows some success in the production of chimeric hydrogenases. However, challenges remain which will likely require further structural modifications or incorporation of additional iron-sulfur clusters to fully realize the desired electron transfer capabilities.

2.3. The Synechocystis reductase module interacts with the C. necator hydrogenase module.

C. necator is a well-established production system for [NiFe]-hydrogenases, allowing the expression not only of its native hydrogenases but also of heterologous SHs from *H. thermoluteus* and *R. opacus*.[28,29] In addition, the reductase module of *Syn*SH was successfully produced in *C. necator*.[9] Previous studies have also shown that *Cn*HoxYH can interact with

reductase modules from SHs of other species.[49] Based on this, we investigated the direct coupling of *Cn*HoxYH to *Syn*HoxEFU using a *C. necator* HF903 strain (Δ*hoxFU*, *Cn*SH$^-$) in which *Cn*HoxFU is deleted and replaced by either plasmid-encoded *Cn*HoxFU (*Cn*SH*) or *Syn*HoxEFU (MixSH).[9,50] As shown previously, purification of the entire MixSH complex is not feasible due to dissociation of the two modules during the process (Figure S9).[9] Therefore, *in vivo* experiments were performed to investigate coupling of *Syn*HoxEFU and *Cn*HoxYH. The successful interaction of the two modules can be demonstrated by (chemolitho)autotrophic growth, which is dependent on a functional SH. Thus, the *Cn*SH$^-$ strain, which lacks the reductase module, is incapable of autotrophic growth. However, this ability can be restored by recombinant production of reductase modules from either *C. necator* or other organisms.[49] Autotrophic growth using H_2 as energy source, CO_2 as carbon source and O_2 as final electron acceptor was observed in the MixSH-producing strain (Figure 3 A), confirming successful electron transfer from *Cn*HoxYH to *Syn*HoxEFU. But, it is noteworthy that colony formation takes approximately two weeks, compared to only five days for the control strain *Cn*SH* under identical growth conditions. As expected, no colonies were observed for the non-reconstituted strain *Cn*SH$^-$. To ensure that the colonies finally formed were not revertants, colony PCR was performed and the fragments separated on an agarose gel showed the expected sizes for both the MixSH and *Cn*SH* strains (Figure S10). Sequencing of the PCR fragments further verified their identity.

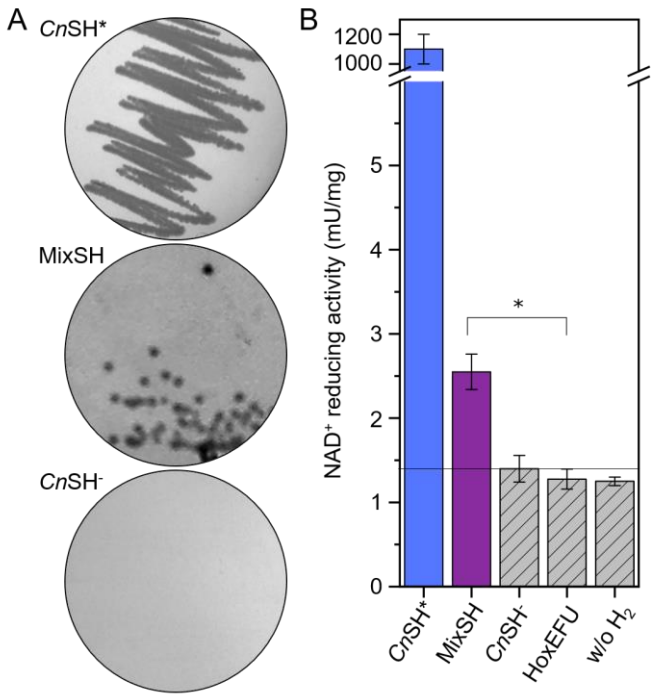


Figure 2) Module interaction of *Syn*HoxEFU and *Cn*HoxYH. A) Lithoautotrophic growth of *C. necator* in an H_2 containing atmosphere. While the *Cn*SH* producing strain forms colonies after 5 days, the MixSH strain forms colonies after two weeks. No colonies are detectable for the reductase deficient strain *Cn*SH$^-$, which produces only *Cn*HoxYH. B) NAD^+ reducing activity in soluble extract of *C. necator* strains producing *Cn*SH* (blue) or MixSH (violet). Only background activity was detectable in soluble extract of *C. necator* strains producing only the *C. necator* hydrogenase module (*Cn*SH$^-$) or the *Synechocystis* reductase module (*Syn*HoxEFU), respectively. Asterisk indicates significant difference between MixSH and *Syn*HoxEFU (p value < 0.05), the horizontal line marks the base line activity.

To further confirm the interaction between the *Syn*HoxEFU and *Cn*HoxYH modules, photometric measurements were performed using soluble cell extracts to assess H_2-driven NAD^+-reducing activity (Figure 3 B). The soluble extract from the MixSH producing strain

showed an apparent specific activity of 2.55 mU mg^{-1}, which is in the same range of previously reported values for a reconstituted SH strain and the wild type (Table S3).[18,50] However, the MixSH activity is approximately twice as high as that observed in extracts from strains producing either the *Cn*HoxYH module alone (*Cn*SH^-, 1.70 mU mg^{-1}) or the *Syn*HoxEFU module alone (1.34 mU mg^{-1}). These values are comparable to the background activity measured in controls without H_2 addition (1.25 mU mg^{-1}). The background activity detected in the controls is probably due to the presence of other NAD^+-reducing enzymes in the soluble extract. Importantly, the activity of the MixSH strain is significantly higher than that of the controls, which is consistent with the results of the lithoautotrophic growth experiments and supports the conclusion that there is a functional interaction between the two modules.

The extended time required for colony formation and low NAD^+-reducing activity of the MixSH strain suggest that electron transfer from *Cn*HoxYH to *Syn*HoxEFU is possible but highly inefficient, likely due to structural mismatches causing poor alignment of iron-sulfur clusters. The known dissociation of HoxYH and HoxEFU in native *Syn*SH further supports weak module interaction, meaning only a small fraction of MixSH complexes are likely functional. Additionally, the simplified production system may limit activity due to constraints in expression and plasmid design. In conclusion, these results demonstrate the possibility of electron transfer from the *C. necator* hydrogenase module to the *Synechocystis* reductase module. Nevertheless, achieving efficient transfer will necessitate targeted structural optimization to stabilize the module interface and facilitate effective electron flow in chimeric hydrogenases.

2.4. Chimeric reductase modules show enhanced interaction with CnHoxYH. To enhance the interaction between *Cn*HoxYH and *Syn*HoxEFU, several modifications were introduced into the *Synechocystis* reductase module, resulting in a series of chimeras (Figure 2). Briefly, in chimera Ch-$HoxEF_{Syn}$+U_{Cn}, the entire HoxU subunit is replaced by *Cn*HoxU, while in Ch-$HoxU^{swapCTD}$, only the CTD of HoxU ($HoxU^{\mathbf{GETTAE}KIGDRRKVEFLATARKEKEWVR\mathbf{211RVGYDDPIGR}KYEIQSVRARALEGEDK}$) was replaced. In chimera Ch-$HoxU^{swap\Phi loop}$, the polar amino acids in the first HoxY-interface region of *Syn*HoxU were substituted by the homologous hydrophobic residues of *Cn*HoxU ($HoxU^{GM\mathbf{DH}SRFKYQFPK\mathbf{119}DM\mathbf{MV}SRFPYRFPV}$), and in chimera Ch-$HoxF^{swapCTD}$, the C-terminal helix of *Cn*HoxF was fused to *Syn*HoxF ($HoxF^{LKV\mathbf{531}VRHEGPLLPSFDLDTALGGYEKALKDLEEVTR}$). All these variants could be purified to good purity (Figure S9) and yielded approximately 3-5 mg from 10 g of cell pellet, wet weight. However, similar to MixSH, purification led to dissociation of the hydrogenase module, with occasional dissociation of the HoxU subunit in the case of Ch-$HoxEF_{Syn}$+U_{Cn}. This dissociation probably results from weak interactions between *Cn*HoxU and *Syn*HoxEF. As the purification process was inconclusive, subsequent *in vivo* studies were performed with the *C. necator* strains carrying the respective chimeras.

Autotrophic growth experiments were performed as described for the MixSH carrying strain. All chimera-bearing strains were incubated in an H_2-containing atmosphere with CO_2 as the sole carbon source. Similar to the MixSH strain, colony formation indicated successful electron transfer from H_2 oxidation at the hydrogenase module to the reductase module, resulting in NADH production. Moreover, as the presence of O_2 as the terminal electron acceptor is essential for the lithoautotrophic growth of *C. necator*,[51,52] the assay also demonstrates the O_2-tolerance of the respective chimeras. Colonies appeared after 5 days on plates with strains containing the *Cn*$SH^{\Delta NTD\text{-}HoxF}$+HoxE and *Cn*SH+HoxE chimeras described above, a growth time comparable to that of the reconstituted *Cn*SH* strain. For strains bearing chimeras Ch-$HoxEF_{Syn}$+U_{Cn} or Ch-$HoxU^{swapCTD}$, colonies were observed after 10 and 14 days respectively, which corresponds to the growth time of the MixSH strain. Notably, all chimera-

bearing strains except the Ch-HoxU$^{swap\Phi loop}$ strain showed a significantly higher number of colonies than the MixSH-bearing *C. necator* strain. In contrast, plates containing the Ch-HoxU$^{swap\Phi loop}$ strain showed few visible colonies after 21 days of incubation (Figure S11).
Spectrophotometric activity measurements were performed on soluble cell extracts from chimera-bearing strains capable of autotrophic growth by following H_2-mediated NAD^+ reduction (Figure 4 A, Table S3). The apparent specific activities of chimeras *Cn*SH$^{\Delta NTD\text{-}HoxF}$+HoxE, *Cn*SH+HoxE and Ch-HoxEF$_{Syn}$+U$_{Cn}$ were significantly higher than those of MixSH, while Ch-HoxU^{swapCTD} exhibited an activity comparable to MixSH. In contrast, modifications in chimera Ch-HoxU$^{swap\Phi loop}$ resulted in a reduced activity compared to MixSH. Among the chimeras, *Cn*SH+HoxE showed the highest apparent specific activity of 85.3 mU mg^{-1}. This was expected as *Cn*SH+HoxE retains the original structure of *Cn*SH with only *Syn*HoxE co-expressed. However, the activity of *Cn*SH+HoxE is an order of magnitude lower than the 1.1 U mg^{-1} determined for soluble extracts of reconstituted *Cn*SH*.[49] This suggests that the presence of *Syn*HoxE has some negative effect on NAD^+ reduction activity *in vivo*. One possibility is that HoxE may structurally compete with the homologues *Cn*HoxF NTD, thereby inducing a suboptimal conformation for electron transfer at the adjacent NAD^+ binding site. Further support for this hypothesis comes from the chimera *Cn*SH$^{\Delta NTD\text{-}HoxF}$+HoxE, in which the *Cn*HoxF NTD is truncated to match the length of *Syn*HoxF, resulting in a further reduced activity of 19.9 mU mg^{-1}. These results highlight the functional importance of the *Cn*HoxF NTD, as previously demonstrated for the homologous HoxE in *Syn*SH.[9,26,53] The reduced protein yield observed during purification further suggests that the *Cn*HoxF NTD contributes to structural integrity. Whether it also directly affects electron transport in *Cn*SH remains speculative and requires further investigation.

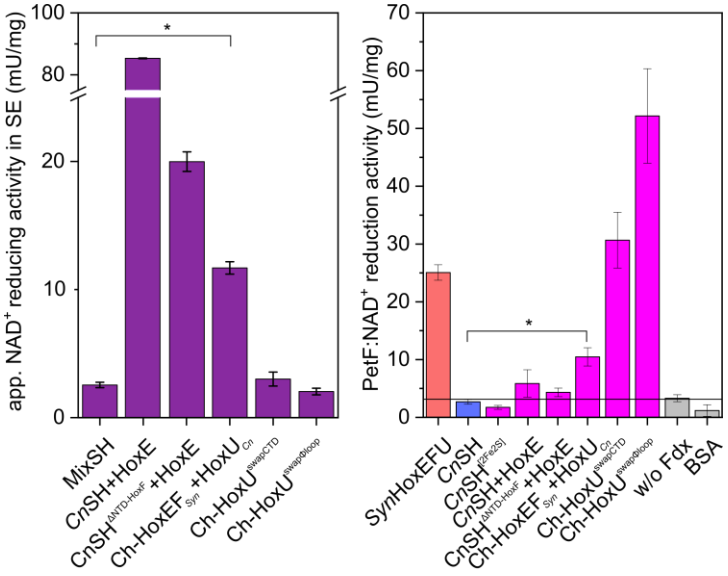


Figure 3) NAD+ reducing activity of chimeric SHs. A) H_2-dependent NAD^+ reducing activity in soluble extract of chimeras-bearing *C. necator* strains (violet). B) Ferredoxin-dependent NAD^+ reducing activity of purified enzymes. In accordance with Figure 2, *Syn*SH is shown in red, *Cn*SH in blue and consequently the chimeric variants in violet. Samples were measured in triplicates; the error bars represent the standard deviation. Asterisks indicate significant difference ($p > 0.05$). Horizontal line indicates background activity determined by negative controls.

The chimera Ch-HoxEF$_{Syn}$+U$_{Cn}$, which combines *Cn*HoxU with *Syn*HoxEF, showed a significantly higher apparent NAD^+-reducing activity in the soluble extract compared to MixSH

(Figure 4 A). The measured activity of 11.7 mU mg^{-1} is four times higher than that of MixSH, indicating that the substitution of the HoxU subunits in Ch-HoxEF$_{Syn}$+U$_{Cn}$ notably improved the electronic coupling between the hydrogenase and reductase modules. In contrast, substitutions involving smaller regions of *Syn*HoxU, as implemented in the Ch-HoxU^{swapCTD} and Ch-HoxU^{swapΦloop} chimeras (Figure 4 A), did not lead to comparable improvements.

The lower activity observed in the chimeras compared to *Cn*SH* is probably due to subunit/module dissociation, which is also supported by the purification results. This probably disrupts the structural integrity and hinders efficient electron transfer between the hydrogenase and reductase modules. It has been reported that the addition of Ni^{2+} and Mg^{2+} ions enhances the coupling between the hydrogenase and reductase modules in bacterial NAD^+-reducing hydrogenases from *R. opacus* (*Ro*SH) and *H. thermoluteus* (*Ht*SH).[28,29,54] Therefore, the influence of Ni^{2+} and Mg^{2+} ions on the chimeras described here was investigated (Figure S12). Contrary to the results observed for *Ro*SH and *Ht*SH, adding Ni^{2+} and Mg^{2+} did neither affect the activity of MixSH nor that of *Cn*SH$^{ΔNTD-HoxF}$+HoxE, *Cn*SH+HoxE and Ch-HoxU^{swapΦloop}. Actually, it was observed that the addition of nickel in particular had a negative effect on the NAD^+-reducing activity. Mg^{2+} on the other hand had either no effect or a slightly positive effect on the activity of *Cn*SH$^{ΔNTD-HoxF}$+HoxE, possibly by stabilizing the interaction with *Syn*HoxE or the structural integrity of the truncated HoxF. Also, the chimera Ch-HoxU^{swapCTD} do not show an increased activity upon addition of Ni^{2+} and/or Mg^{2+}, but a significant prolongation of the reaction was observed. Surprisingly, the addition of Ni^{2+} and Mg^{2+} has an activity-enhancing effect on the activity of Ch-HoxEF$_{Syn}$+U$_{Cn}$ (*Syn*HoxEF + *Cn*HoxUYH). The addition of Ni^{2+} and Mg^{2+} increases the activity from 11.7 mU mg^{-1} to 51.8 mU mg^{-1}, which is 20 times higher than the NAD^+-reductase activity determined for MixSH. It also exceeds the activities determined for *Cn*SH$^{ΔNTD-HoxF}$+HoxE and approaches the activities determined for *Cn*SH+HoxE. Since the HoxU subunit in Ch-HoxEF$_{Syn}$+U$_{Cn}$ originates from *Cn*SH, this effect is probably due to an improved coupling of the subunits within the reductase module, where Ni^{2+} and Mg^{2+} ions may bind to surface regions of HoxU or HoxF, inducing conformational changes that enhance contact within HoxFU. Furthermore, these ions may contribute to the formation of a stabilizing network of ionic and hydrogen bonds between modules/subunits. However, for *Syn*HoxEFU and most of the chimeras described here, a positive effect of Ni^{2+} and Mg^{2+} on the coupling of the two modules, as in *Ro*SH and *Ht*SH, does not seem to be transferable.[28,29,54] Finally, three chimeric reductase modules could be identified which show an improved electron transfer from the hydrogenase module. Their ability to interact with ferredoxin, one of the key features for photosynthesis-coupled H_2 production, was therefore of particular interest.

Therefore, the ferredoxin interaction was assessed by photometric measurements monitoring the reduced ferredoxin Fdx_{red}-dependent NAD^+ reduction (Figure 4 B). Activity measurements based on reduced ferredoxin are challenging without a recycling system to maintain a sufficient supply of reduced ferredoxin for a sustained reaction. Sodium dithionite (DT) is commonly used as a recycling agent to facilitate monitoring of ferredoxin-dependent H_2 production.[1] But since DT also can transfer electrons directly to hydrogenases, this method is prone to false-positive results. An alternative recycling system uses pyruvate ferredoxin oxidoreductase (PFOR) to regenerate reduced ferredoxin. Unfortunately, this method is not suitable for soluble extracts because the presence of the pyruvate dehydrogenase (PDH) in soluble extracts leads to the production of NADH, which causes false-positive results.[55] However, as the monitored reaction does not require a hydrogenase module, purified reductase modules were used to eliminate side reactions of PDH. Background activity was assessed using negative controls where either ferredoxin was not added or bovine serum albumin (BSA) was used instead of a hydrogenase. Consistent with previous findings,

ferredoxin interaction was observed for the wild-type *Syn*HoxEFU module (25.1 mU mg^{-1}) but not for *Cn*SH, which was below the cut-of value of 3.3 mU mg^{-1}. As considered above, the introduction of an additional [2Fe2S]^{F2} cluster in *Cn*SH (*Cn*SH$^{[2Fe2S]}$) was not sufficient to enable ferredoxin interaction. Similarly, the modifications in chimeric hydrogenases *Cn*SH$^{\Delta NTD\text{-}HoxF}$+HoxE and *Cn*SH+HoxE did not provide ferredoxin interaction, as expected. However, chimeras Ch-HoxEF$_{Syn}$+U$_{Cn}$, Ch-HoxU^{swapCTD} and Ch-HoxU$^{swap\Phi loop}$, which retain more elements of the original *Syn*HoxEFU module, successfully exhibited ferredoxin interaction, 10.5, 30.7 and 52.2 mU mg^{-1} respectively. While Ch-HoxEF$_{Syn}$+U$_{Cn}$ shows slightly lower activity than *Syn*HoxEFU, Ch-HoxU^{swapCTD} and Ch-HoxU$^{swap\Phi loop}$ exhibit even higher values. However, the increase in Ch-HoxU^{swapCTD} is not statistically significant and Ch-HoxU$^{swap\Phi loop}$ is marked by high variability between replicates, as reflected in a large standard deviation. The reduced activity of Ch-HoxEF$_{Syn}$+U$_{Cn}$ is most likely due to by compromised structural integrity, as evidenced by the loss of HoxU subunit during purification and appearance of a strong 65 kDa band, associated with DnaK (Figure S9).[48] Nevertheless, Ch-HoxEF$_{Syn}$+U$_{Cn}$ still accepts electrons from ferredoxin, despite it lacks the [4Fe4S]^{U4} cluster of *Syn*HoxU. The [4Fe4S]^{U4} cluster has been proposed as one of the three potential ferredoxin interaction sites in *Syn*SH, alongside the [2Fe2S] clusters in HoxE and HoxF.[25] However, previous docking studies have ruled out [2Fe2S]E1 as a likely ferredoxin-interaction site,[9] suggesting instead that it acts as a redox-gated switch that regulates electron flow within the reductase module.[56] This supports the conclusion that HoxF, and specifically the [2Fe2S]^{F2} cluster, plays crucial role in electron acceptance from ferredoxin. Due to the reduced activity in comparison of *Syn*HoxEFU, a second ferredoxin binding site on HoxU cannot be excluded. However, AlphaFold models of the homodimeric *Syn*SH suggest, that the [4Fe4S]^{U4} is blocked by dimerization.[9,57] Together with the results from the module interaction assays, this indicates that MixSH, Ch-HoxEF$_{Syn}$+U$_{Cn}$ and Ch-HoxU^{swapCTD} are the only chimeras that can both interact with the O_2-tolerant hydrogenase module of *Cn*SH and accept electrons from reduced ferredoxin, both essential for photosynthesis-coupled H_2 production. In conclusion, this study has successfully developed chimeric hydrogenases that combine the essential properties for photosynthesis coupled H_2 production: O_2 tolerance and ferredoxin interaction. Furthermore, we have identified a ferredoxin binding site in *Syn*SH at HoxF. The chimeras developed here were subsequently transferred into *Synechocystis* to test their ability for photosynthesis-coupled H_2 production.

2.5. Evaluation of chimeric hydrogenases in Synechocystis.

To evaluate the functionality of chimeric hydrogenases in *Synechocystis*, we initially constructed mutant strains by genomic integration of chimeric constructs *Syn*_MixSH and *Syn_Cn*SH$^{HoxEF\text{-}fusion}$, since the other chimeric hydrogenases were developed at a later stage of the study. A detailed description can be found in the Supplementary Information I. Briefly, the chimeric hydrogenases were produced under the control of the constitutive promoter P$_{psbA2}$ into a Δ*hox* background (*Syn*_Δhox') alongside control strains (*Syn_Cn*SH and *Syn*_HoxYH$_{Cn}$). Integration was confirmed by PCR (Figure S13) and immunoblot analysis (Figure S14), which showed robust expression of *Syn*HoxE and *Syn*HoxF in *Syn*_MixSH, whereas *Syn_Cn*SH$^{HoxEF\text{-}fusion}$ produced the expected *Syn*HoxE-*Cn*HoxF fusion protein. However, *in vivo* gas chromatography measurements revealed that only *Syn_Cn*SH and *Syn_Cn*SH$^{HoxEF\text{-}fusion}$ exhibited significant H_2 consumption, whereas no activity was detected for *Syn*_MixSH (Figure S15). In accordance with this, H_2 production capacity using an artificial electron donor was only detected for *Syn_Cn*SH and *Syn_Cn*SH$^{HoxEF\text{-}fusion}$ (Figure 5 A). *Syn*_MixSH in contrast

showed low but not significant activity. However, importantly, all three strains were able to produce H_2 under fermentative conditions, yet, none of them was capable of prolonged photo-H_2 production after a switch to light (Figure 5 B, S16). Notably, the quantities of fermentative H_2 produced by *Syn*_MixSH were low compared to the other strains, thus indicating an activity of this chimeric variant close to the limit of detection. In general, the overall activities of the hydrogenases remained very low compared to *C. necator*. This suggests that only low proportions of fully maturated and active hydrogenase are present in *Synechocystis*.

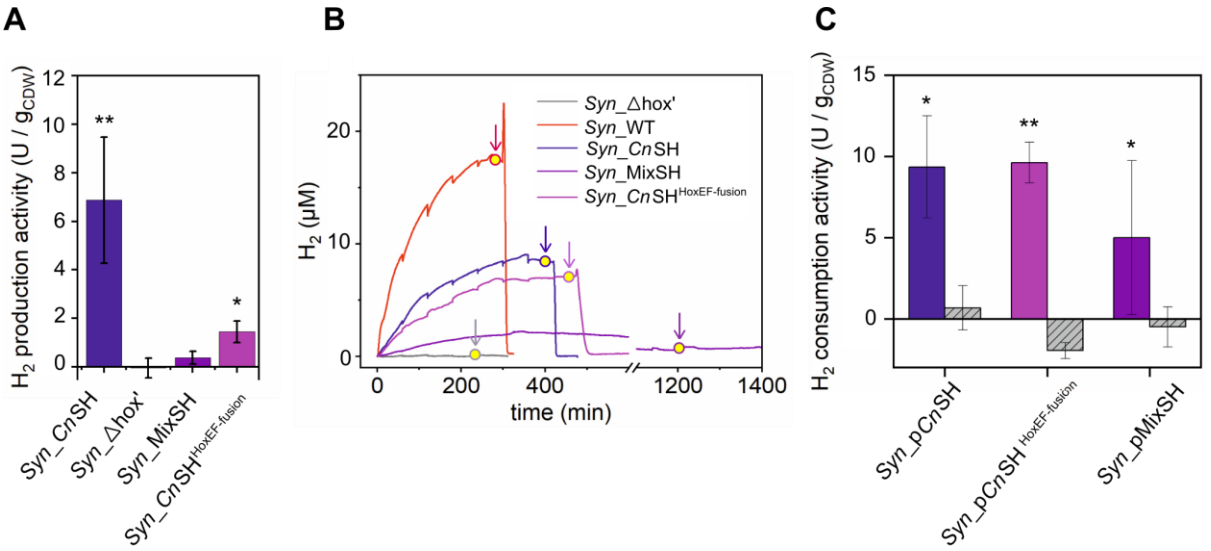


Figure 5) Activity of chimeric SHs in *Synechocystis* sp. PCC 6803. A) Specific H_2 production activities of *Syn_Cn*SH, *Syn*_Δhox', *Syn*_MixSH and *Syn_Cn*SH$^{HoxEF\text{-}fusion}$ cultures using dithionite-reduced methyl viologen (MV) as an artificial electron donor. H_2 production was analyzed *in vivo* using a Clark-type electrode. Specific H_2 production activities given in units per g cell dry weight (U / g_{CDW}) were calculated from the increase in H_2 within the linear range and calculated from the signal slope in the range of linear H_2 increase and normalized by subtraction of the mean H_2 turnover of the reference strain *Syn*_Δhox'. 1 U is defined as the production of 1 µmol H_2 min^{-1}. All values are means ± standard deviations of 5-6 biological replicates. Welch-ANOVA of specific activities followed by a post-hoc Games-Howell comparison test ($P < 0.05$) resulted in F (9.583; 3) = 20.695; $p < 0.001$. Asterisks indicate significant differences of $p < 0.05$ (*) or $p < 0.01$ (**). A detailed itemization of the P values is appended in Statistics S3. B) H_2 production of *Syn*_Δhox', Syn_WT, *Syn_Cn*SH, *Syn*_MixSH and *Syn_Cn*SH$^{HoxEF\text{-}fusion}$ under fermentative and photosynthetic conditions measured via Unisense electrode. Fermentative conditions were generated by the addition of 10 mM glucose, 40 U / ml glucose oxidase and 50 U / ml catalase and incubation in the dark. Photosynthetic conditions were generated by a sudden switch to light (750 µE / m^2 / s); the corresponding time points are indicated by arrows and yellow spheres. C) Specific H_2 consumption activities of *Syn*_p*Cn*SH, *Syn*_pMixSH and *Syn*_p*Cn*SH$^{HoxEF\text{-}fusion}$ obtained from GC analysis after 6 h of incubation with 20% H_2, 10% CO_2, and 70% N_2 in sealed 20 ml glass vials and in the presence of light. Strains were pre-grown photoautotrophically and induced with 2.5 µM Ni^{2+} for 24 h (filled bars) or grown without induction (dashed, grey bars). 1 U is defined as the consumption of 1 µmol H_2 min^{-1}. Values are means ± standard deviations of biological duplicates (uninduced) or triplicates (induced). Asterisks indicate significant differences of $p < 0.05$ (*) or $p < 0.01$ (**) between induced and uninduced approaches obtained from 2-sample t-tests.

Building on these findings, we explored an alternative expression strategy for the advanced chimeric hydrogenases (*Cn*SH$^{\Delta NTD\text{-}HoxF}$+HoxE, *Cn*SH+HoxE, Ch-HoxEF$_{Syn}$+U$_{Cn}$ and Ch-HoxU^{swapCTD}) as well as MixSH, *Cn*SH$^{HoxEF\text{-}fusion}$ and *Cn*SH. Instead of genomic integration, these constructs were expressed from a replicative plasmid under the control of the Ni^{2+}-inducible promoter P_{nrsB},[58] in combination with a highly efficient ribosome binding site (RBS*: TAGTGGAGGT),[59] which was shown to enhance hydrogenase activity.[31] Additionally, an alternative *hox* deletion strain (*Syn*_Δhox) was used as a parental strain, as it has been shown to support improved H_2 production under similar conditions.[31] The obtained strains

*Syn*_p*Cn*SH, *Syn*_pMixSH, *Syn*_p*Cn*SH$^{HoxEF\text{-}fusion}$, *Syn*_p*Cn*SH$^{\Delta NTD\text{-}HoxF}$+HoxE, *Syn*_p*Cn*SH+HoxE, *Syn*_pCh-HoxEF$_{Syn}$+U$_{Cn}$ and *Syn*_pCh-HoxU^{swapCTD} were verified by PCR (Figure S17). Expression of *hox* genes was analyzed via immunoblotting using antibodies α-*Syn*HoxE, α-*Syn*HoxF, α-*Cn*HoxH (Figure S18).[60] For hybridization with α-*Cn*HoxH, all cyanobacterial chimeric strains induced with either 2.5 or 10 µM Ni^{2+} yielded a signal of the expected size (lanes 9-15), while no signal was detected for strains grown without induction (lanes 4 and 8). Consequently, expression of the hydrogenase module in those strains can be assumed, albeit the expression was lower than for strains expressing the *Cn*SH (lane 5-7). This circumstance may be attributed to the distance of *hoxYH* from the promoter,[61] as the genes encoding the subunits of the chimeric reductase module, such as *hoxEFU* from *Synechocystis*, are larger than *hoxFU* from *C. necator*. Production of the reductase module was investigated by hybridization with α-*Syn*HoxE and α-*Syn*HoxF.[60] Notably, both antibodies yielded cross-reactive signals with the respective other protein (Figure S18 B/C). For hybridization with α-*Syn*HoxE, production of the 18.8 kDa HoxE was observed for all cyanobacterial chimera strains induced with either 2.5 or 10 µM Ni^{2+} (lane 9-15) but the signal for *Syn*_pCh-HoxEF$_{Syn}$+U$_{Cn}$ was particularly weak (lane 12). This may be due to lower expression levels compared to other chimeric variants or instability of the chimeric hydrogenase enzyme in *Synechocystis*.[62] Surprisingly, neither HoxE nor HoxF was detected in the *Syn*_WT sample (lane 2), for reasons that are unclear, but may be due to lower expression under the native promoter. Inhomogeneous protein concentrations in the loaded extracts can be excluded (Figure S18 A). In addition, *Syn*HoxF was not detectable in the chimeric variants either, except in the Ni^{2+}-induced *Syn*_pMixSH (Figure S18 C). Among the chimeric versions, no signal from hybridization with α-*Syn*HoxF was expected for *Syn*_p*Cn*SH$^{\Delta NTD\text{-}HoxF}$+HoxE and *Syn*_p*Cn*SH+HoxE as they carry the gene encoding *Cn*HoxF. However, *Syn*_pCh-HoxEF$_{Syn}$+U$_{Cn}$ and *Syn*_pCh-HoxU^{swapCTD} were expected to give a signal at 57.8 kDa for *Syn*HoxF. In fact, this was not the case. It is therefore most likely that the protein expression or the maturation was hampered and no functional protein was produced. Possible explanations are either a to low expression or instability of the chimeric versions in *Synechocystis*.[62] However, considering the fact that *hoxE* and the downstream-located *hoxH* are expressed in those strains, it is likely that those strains produce at least low quantities of the chimeric hydrogenases.

To investigate the hydrogenase activity of the newly generated strains, H_2 consumption was determined by GC analysis. Pre-grown liquid cultures of all strains and the corresponding control strains were flushed with 20% H_2, 10% CO_2, and 70% N_2 and incubated in sealed glass vials under continuous illumination. H_2 consumption was analyzed via GC immediately after flushing with the gas mixture as well as after 2 h, 4 h, 6 h and 8 h of incubation. However, except for *Syn*_p*Cn*SH**,** activity was only observed within the first 6h of incubation (Table S4). Cultures induced with 2.5 µM Ni^{2+} for 24 h and cultures grown without induction were compared for all strains. To allow a better comparison with cyanobacterial strains bearing genomic integrated chimeric hydrogenases, H_2 consumption activities for the whole time from flushing until 6h of incubation were calculated. Apparently elevated activities for the Ni^{2+}-induced versus uninduced samples were observed for *Syn*_p*Cn*SH, *Syn*_pMixSH and *Syn*_p*Cn*SH$^{HoxEF\text{-}fusion}$ (Figure 5 C). In contrast, no activities were observed for the advanced chimeric hydrogenases *Cn*SH$^{\Delta NTD\text{-}HoxF}$+HoxE, *Cn*SH+HoxE, Ch-HoxEF$_{Syn}$+U$_{Cn}$ and Ch-HoxU^{swapCTD} (Table S4). This is most likely due to hampered protein expression or maturation, as identified in the Western blots (Figure S18 B/C). Among the strains showing H_2 consumption activity, *Syn*_p*Cn*SH and *Syn*_p*Cn*SH$^{HoxEF\text{-}fusion}$ are almost identical (Figure 5 C, Table S4). The activity of *Syn*_pMixSH showed a high variance between the replicates and was lower but significant compared to the uninduced approach, indicating that the chimera enzyme is functionally produced in *Synechocystis*. Notably, the observed specific activities

were even higher than for strains bearing the respective genomic integrated version (Figure 5 C, Table S4), thus confirming the improved hydrogenase production from the P_{nrsB}-RBS* expression system. To summarize, *Cn*SH, MixSH and *Cn*SH$^{HoxEF\text{-}fusion}$ recombinantly produced on a replicative plasmid show a low H_2 consumption activity in *Synechocystis*. Recently we improved *Cn*SH activity by additionally expressing the maturation system of *C. necator* in *Synechocystis* - this approach could also improve enzyme activities of the chimeric enzymes.[31]

Together, these results demonstrate that, despite current limitations, the modular chimeric hydrogenase design has promising potential for photosynthesis-driven H_2 production in *Synechocystis*, as evidenced by the H_2 consumption activity observed for *Cn*SH and *Cn*SH$^{HoxEF\text{-}fusion}$ as well as fermentative H_2 production activity obtained for *Cn*SH, *Cn*SH$^{HoxEF\text{-}fusion}$ and MixSH upon genomic integration. Moreover, the activity of chimeric hydrogenases was further enhanced when expressed from a replicative plasmid, allowing H_2 consumption to be detected also in MixSH.

3. Conclusion

In this study, we have demonstrated the feasibility of engineering chimeric hydrogenases by combining modules from *C. necator* and *Synechocystis* sp. PCC 6803 to enable oxygen tolerance and interaction with photosynthetic electron carriers, both essential for photosynthesis-driven H_2 production. Additionally, our findings reveal a ferredoxin binding site on HoxF in *Syn*SH. Among the different chimeric constructs investigated, strains harbouring the *Syn*HoxEFU and *Cn*HoxYH modules - especially those corresponding to the MixSH and Ch-HoxEF$_{Syn}$+U$_{Cn}$ variants - exhibited measurable H_2 consumption activity under aerobic conditions in *C. necator* and partly also in *Synechocystis*. These activities indicate electronic coupling between the H_2 converting [NiFe] active site and the cofactor binding sites at the reductase module. Moreover, these variants also showed the ability of ferredoxin interaction. However, despite these promising results, the overall hydrogenase activity in *Synechocystis* remains significantly lower than that observed in *C. necator*, with the corresponding activity in the heterologous host reduced by several orders of magnitude. This substantial reduction appears to be due to a combination of factors, including host specific features, suboptimal expression levels, poor enzyme stability and incomplete maturation of the chimeric hydrogenases in the cyanobacterial system. The variability in expression and inconsistent detection of key hydrogenase subunits, particularly HoxF, highlights the challenges of stabilizing these complex multi-subunit enzymes in a heterologous host. In particular, the use of a replicative plasmid expression system with an inducible promoter improved expression in some cases, however, this strategy still failed to achieve the levels of activity required for efficient photosynthetic H_2 production but provides as base for further approaches.

In summary, although our modular hydrogenase design successfully enables partial hydrogenase activity in *Synechocystis* as demonstrated by both H_2 consumption and fermentative H_2 production, significant hurdles remain. Achieving efficient and robust photosynthesis-driven H_2 production in cyanobacteria will likely require further optimization of the expression system, improved assembly and maturation of the chimeric enzymes, and refined structural integration to ensure effective electron transfer between modules. These findings provide valuable insights and a solid foundation for future efforts to improve the

stability and activity of engineered hydrogenases, ultimately contributing to the development of sustainable biohydrogen production platforms.

4. Experimental Materials and Methods

4.1. Strains and growth conditions. All strains used in this study are summarized in supplementary Table S5. *Escherichia coli* strains DH5α,[63] DH10β and TOP10 (Invitrogen, Life Technologies, Paisley, UK) were grown at 37°C in liquid Luria broth (LB) medium shaking at 130–200 rpm or on LB agar plates. The medium was supplemented with either 50-100 µg mL^{-1} spectinomycin or 50 µg mL^{-1} kanamycin.

C. necator strains were grown in either fructose-nitrate (FN) minimal medium, fructose-glycerol-nitrate (FGN) minimal medium or autotrophic-nitrate (AutN) minimal medium.[64] All based on phosphate buffer H16 (25 mM Na_2HPO_4 and 11 mM KH_2PO_4, pH 7.0) supplemented with 0.2% (w/v), NH_4Cl, 0.81 mM $MgSO_4$, 0.068 mM $CaCl_2$, 18 µM $FeCl_3$, and 1 µM $_2$ (AutN). No organic carbon source was added to the AutN minimal medium, FN minimal medium additionally contained 0.4% (w/v) fructose, whereas FGN minimal medium additionally contained 0.05% (w/v) fructose and 0.4% (w/v) glycerol. *C. necator* cultures harboring plasmids were supplemented with 200-750 µg mL^{-1} kanamycin.

Cyanobacterial strains were grown photoautotrophically in yBG11 liquid medium,[65] buffered with 50 mM HEPES, pH 7.2. If not specified otherwise, cultivation was performed in baffled shaking flasks with cotton plugs at 30°C, light intensities of 25-50 µmol photons m^{-2} s^{-1}, ambient (0.04%) CO_2, 75% humidity and 150 rpm. Growth on BG11 agar plates[66] was conducted at the same conditions, but without shaking. If required, antibiotics were added to final concentrations of 50 and 40 µg mL^{-1} for kanamycin and spectinomycin, respectively. For expression of *hox* genes under the control of P_{psbA2}, the medium was supplemented with 17 µM ferric ammonium citrate and 1 µM $NiCl_2$ to support hydrogenase assembly and activity.[67] For expression of *hox* genes under the control of P_{nrsB}, the expression was induced with 2.5-10 µM Ni^{2+} for 24-48h.

4.2. Plasmid construction for chimeric hydrogenases. For heterologous production of chimeric hydrogenases in *C. necator* HF903,[50] all constructs were cloned into either plasmid pJP66 (Figure S19 A) or pLL9010.40 (Figure S19 B).[9] Both are based on the plasmid pCM66[68] and additionally contain the SH promoter from *C. necator*[69] and a StrepTagII® coding region for purification, as well as the genes for the reductase modules from *C. necator* (*Cn*hoxFU) or *Synechocystis* sp. PCC6803 (*Syn*hoxEFU), respectively (Table S6). Phusion® High Fidelity DNA Polymerase (New England Biolabs®, Germany) was used to amplify the DNA fragments. All oligos used for amplification of DNA fragments are listed in supplementary Table S7 and the sequences of all plasmids are compiled in the supplementary information 3.

For construction of the *Cn*HoxF derivative with an additional $[2Fe2S]^{E1}$ cluster, the bases of *CnhoxF* 2689 to 2694 and 2809 to 2823 were substituted with primers 2Fe2S_IA79AC and 2Fe2S_LSDQE119ACGIA, finally resulted in plasmid pLL297_91. Plasmids pEL9111, pEL03, pEL26 and pEL35 were generated using the assembly protocol described by Gibson.[70] The plasmids pEL25, pEL42 and pEL44 were constructed through a kinase-ligase reaction (KDL Enzyme Mix, New England Biolabs). Plasmid pEL9111 was constructed by amplification of the *hoxE* encoding region from pLL9010.40 using primers EL-hoxE-fw/rev and inserted into vector pJP66 linearized by EL-vector-fw/rev. For plasmid pEL03, a 753 bp fragment of pJP66 containing the *CnhoxU* gene, amplified with primers EL932/EL933, was inserted into plasmid

pLL9010.40, linearized with primers EL930/EL931. Plasmid pEL26 was created by inserting a 576 bp fragment amplified with primers EL011/EL012 containing the *SynhoxE* gene into plasmid pJP66 linearized with primers EL009/EL010. Plasmids pEL25 were constructed using primers EL25fw/EL25rev on plasmid pEL26 as template. For plasmid pEL35, a 2434 bp long fragment of pJP66 amplified by EL023/EL024 was substituted into pLL9010.40, linearized by EL021/EL022. Plasmids pEL42 and pEL43 were generated using primers EL01fw/EL01rev on plasmid pLL9010.40 and pEL35 as templates, respectively. Plasmid pEL44 was generated using primers EL28fw/EL28rev on pLL9010.40. Plasmids were transformed into *E. coli* DH10β by heat shock and spread on LB agar plates containing 50 µg/mL kanamycin for selection. The correct cloning of the plasmids was verified by sequencing (Microsynth Seqlab, Göttingen, Germany). Subsequently, they were transformed by electroporation into HoxFU-deficient *C. necator* strain HF903 and hydrogenase-deficient *C. neactor* strain HF1054,[71] respectively.

Both, for generation of replicative plasmids and constructs for integration into the genome of *Synechocystis*, DNA amplification was performed using Q5 High-Fidelity DNA Polymerase (New England Biolabs). Test PCRs for candidate screening were performed applying GoTaq (Promega, USA), Dream Taq (Thermo Fisher Scientific) or OneTaq (New England Biolabs). Restriction enzymes, Fast alkaline phosphatase and the corresponding buffers were purchased from either Thermo Fisher Scientific (Waltham, USA) or New England Biolabs. All final constructs were verified by sequencing at Genewiz (Genewiz Germany GmbH, Germany) or Microsynth Seqlab. Oligos used for amplification and the obtained plasmids are listed in Table S7 and S6, respectively, and the sequences of all plasmids are compiled in the supplementary information 3.

For generation of the construct for integration of *CnhoxYHW* into the genome of *Synechocystis* sp. PCC 6803 (i.e. pHyd_GI), a 5394 bp DNA fragment including the vector backbone, the 5' and 3' homologous regions of the *hox* locus in *Synechocystis*, a spectinomycin resistance cassette and the T_{psbC} terminator was amplified from the plasmid pGGC212 [31] using the primers pGGC-term_for and pGGC-5'_rev. Furthermore, 497 bp P_{psbA2} and 2595 bp *CnhoxYHW* DNA fragments were amplified from chromosomal DNA of *Synechocystis* and pGGC212, respectively, using the primers PpsbA2-NheI-O5hox _for and PpsbA2_rev (P_{psbA2}) or HoxY-OPsbA2_for and HoxW-NotI-OTerm_rev (*CnhoxYHW*). The 497 bp P_{psbA2} fragment was extracted from a 1.5% agarose gel. The PCR products of *CnhoxYHW* and the 5394 bp vector backbone were purified, digested with *Dpn*I and purified again. The vector backbone fragment, P_{psbA2} and *CnhoxYHW* were interconnected via Gibson assembly[70] according to the manufacturer's instructions and transformed into *E. coli* DH5α via electroporation.

Generation of constructs for integration of chimeric hydrogenase versions MixSH and *Cn*SH$^{HoxEF\text{-}fusion}$ into the genome of *Synechocystis* was performed in two steps. In a first step, *Cn*hoxYHW was amplified from pGGC212 via PCR using the primers HoxY-NheI-O5hox_for and HoxW-NotI-OTerm_rev. The 2665 bp PCR product was purified, digested with *Dpn*I and purified again. The *CnhoxYHW* DNA fragment and the 5394 bp vector backbone (also containing the 5' and 3' *hox* homologous regions, a spectinomycin resistance cassette and the T_{psbC} terminator) described above were assembled and transformed in *E. coli* DH5α as outlined before, yielding the plasmid pGGC-Hyd. For the second cloning step, pGGC-Hyd was digested with NheI, dephosphorylated using Fast alkaline phosphatase and purified. Coding sequences of the reductase subunits for the chimeric version MixSH and *Cn*SH$^{HoxEF\text{-}fusion}$ were amplified from the plasmids pLL9010.40 or pEL9111 using the primers HoxE-syn-OPpsbA2_for and HoxU-rals-NheI-OHoxY_rev, yielding PCR-products of 3652 bp and 3075 bp in size, respectively. The 487 bp P_{psbA2} DNA fragment was prepared as described above. For generation of the final constructs pMixSH_GI and pCh-2_GI, the three components (i.e. vector

backbone pGGC-Hyd, P_{psbA2} and the respective reductase subunit) were again ligated via Gibson assembly and transformed into *E. coli* DH5α via electroporation.

For construction of replicative plasmids for transformation into *Synechocystis* sp. PCC 6803, the chimeric versions MixSH, *Cn*SH$^{HoxEF\text{-}fusion}$, *Cn*SH$^{\Delta NTD\text{-}HoxF}$+HoxE, *Cn*SH+HoxE, Ch-HoxEF$_{Syn}$+U$_{Cn}$, and Ch-HoxU^{swapCTD} as well as *Cn*SH (i.e. *hoxFUYHW* from *C. necator*) were fused to the *nrsB* promoter and introduced into the replicative plasmid pSEVA451.[72] To this end, pSEVA451 was linearized by digestion with HindIII, dephosphorylated using Shrimp alkaline Phosphatase (New England Biolabs) and purified. For the chimeric variants MixSH, *Cn*SH$^{HoxEF\text{-}fusion}$ and *Cn*SH, the respective reductase subunits fused to P_{nrsB} and the ribosomal binding site RBS* (P_{nrsB}-RBS*) were amplified from the previously generated plasmids pHoxEFU_MixSH, pHoxEFU_Ch-2, and pCnHoxFU. The primers PnrsB_HindIII-OpSEVA_for and HoxU-syn-NheI-OHoxY_rev (MixSH), PnrsB_HindIII-OpSEVA_for and HoxU-rals-NheI-OHoxY_rev (*Cn*SH$^{HoxEF\text{-}fusion}$) or PnrsB_HindIII-OpSEVA_for and HoxU-rals_OHoxY (*Cn*SH) were applied and PCR-products of 3835 bp, 3230 bp and 2943 bp in length were obtained. For the Hox chimeric versions *Cn*SH$^{\Delta NTD\text{-}HoxF}$+HoxE, *Cn*SH+HoxE, Ch-HoxEF$_{Syn}$+U$_{Cn}$, and Ch-HoxU^{swapCTD}, the reductase subunits and P_{nrsB}-RBS* were prepared from separate PCRs. The respective reductase subunits were amplified from pEL25, pEL26, pEL03 and pEL35 using the primers HoxE-Syn-OPnrsB_for and HoxU-rals-NheI-OHoxY_rev. The obtained PCR-products were 2997 bp (*Cn*SH$^{\Delta NTD\text{-}HoxF}$+HoxE), 3144 bp (*Cn*SH+HoxE), 3668 bp (Ch-HoxEF$_{Syn}$+U$_{Cn}$) and 3661 bp (Ch-HoxU^{swapCTD}) in length. P_{nrsB}-RBS* was amplified from pGGC212 using the primer PnrsB_HindIII-OpSEVA_for and PnrsB-RBS*_rev, yielding a 183 bp DNA fragment. Moreover, a 2847 bp PCR-product covering *CnhoxYHW* and the terminator T_{psbC} was generated using the primers HoxY_for and TpsbC-OpSEVA_rev and pMixSH_GI as a template. The PCR products were either extracted from a gel or purified, digested with DpnI and purified again. The final plasmids p*Cn*SH_R (*Cn*SH), pMixSH_R (MixSH), pCh-2_R (*Cn*SH$^{HoxEF\text{-}fusion)}$, pCh-25_R (*Cn*SH$^{\Delta NTD\text{-}HoxF}$+HoxE), pCh-26_R (*Cn*SH+HoxE), pCh-30_R (Ch-HoxEF$_{Syn}$+U$_{Cn}$), and pCh-35 (Ch-HoxU^{swapCTD}) were generated by assembling the respective components (i.e. pSEVA451 backbone, P_{nrsB}-RBS*, *hox(E)FU* and *HoxYHW*-T_{psbC}) via Gibson Assembly using NEBuilder Hifi DNA Assembly Cloning KIT (New England Biolabs) according to the manufacturer's instructions and subsequent heat-shock transformation into *E. coli* TOP10.

4.3. Construction of cyanobacterial mutant strains. For generation of the cyanobacterial mutant strains *Syn*_HoxYH$_{Cn}$, *Syn*_MixSH and *Syn_Cn*SH$^{HoxEF\text{-}fusion}$, the respective *hox* expression cassettes were integrated into the genome of *Syn*_Δhox', i.e. a *Synechocystis* sp. PCC 6803 strain in which the *hox* genes had been deleted and replaced by a kanamycin resistance cassette.[14] Genomic integration of the *hox* expression cassettes was directed to the *hox* locus, thereby replacing the kanamycin resistance in *Syn*_Δhox' by the expression cassette and a spectinomycin resistance marker. For genomic integration, the plasmids pHyd_GI, pMixSH_GI and p*Cn*SH$^{HoxEF\text{-}fusion}$_GI were introduced into *Syn*_Δhox' via natural transformation according to standard protocols essentially as described by Lupacchini et al.[30] Briefly, for each transformation approach, 100 ml liquid culture were inoculated to an OD_{750} of 0.2 and grown overnight as described above to an OD_{750} of approximately 0.4. The cells were harvested, resuspended in 1 ml yBG11 medium and pelleted again. Finally, the cells were resuspended in 400 µl yBG11 medium and supplemented with 4 µg plasmid DNA. After incubation in the dark at 30 °C for 5 h (with a short hand shaking every 2 h), the suspension was spread on nylon membrane filters (Cytiva, MA, USA), placed on yBG11 agar plates without antibiotics (100 µl suspension per plate), and incubated at 30 °C and 25 µmol photons m^{-2} s^{-1} overnight. Subsequently, the membranes were moved to a fresh agar plates containing the selective antibiotics at 50% of the normal operating concentrations (i.e. 20 µg/ml

spectinomycin). Alternatively, 200 µl of the transformation approach were incubated in the dark overnight, and then directly plated on yBG11 agar plates containing 20% of the normal operating concentration (i.e. 8 µg/ml spectinomycin). After incubation at 25 µmol photons m^{-2} s^{-1} overnight, all plates were transferred to 50 µmol photons m^{-2} s^{-1} and further incubated for 2-3 weeks until single colonies appeared. Candidates strains were spread on fresh agar plates containing increased antibiotics concentrations several times, until fully segregated mutant strains were obtained. The mutant strains were verified by test-PCR, using the primers HoxH_for and Hox-locus_rev for amplification of a 3579 bp mutant-specific DNA fragment (Figure S13 A). Total elimination of parental chromosome versions in fully segregated strains was tested via PCR using the primers Hox-flank_for and Hox-locus_rev (Figure S13 B). In any case, GoTaq polymerase (Promega) was applied. Genomic DNA (gDNA) used as a template for the PCR was isolated by phenol-chloroform extraction according to a universal extraction protocol,[73] but with slight modifications as follows. 10^7-10^8 cells were harvested by centrifugation (10,000 g, 5min, 4 °C) and the cell pellet was resuspended in 467 µl TE buffer. The cells were lysed by the addition of 100 µl lysozyme (10 mg/ml), incubation on a thermomixer at 37 °C for 30 min (shaking at 500 rpm), addition of 15 µl 20% SDS, and incubation for another 30 min under the same conditions. Subsequently, 10 µl proteinase K (20 mg/ml) and 6 µl RNaseA (10 mg/ml) were added and the mixture was incubated for 1 h at 37 °C (shaking at 500 rpm). Next, 100 µl pre-heated 5 M NaCl and 80 µl pre-heated 10% cetyltrimethylammonium bromide (CTAB) in 0.7 M NaCl were added, and the samples were incubated at 65 °C for 20 min on a thermomixer. An equal volume phenol/chlorophorm/isoamyl alcohol (25:24:1) was added. The samples were mixed well and centrifuged for 15 min at 13,000 g and 4 °C. Twice, the upper phase was transferred to a new tube, supplemented with an equal volume of chloroform/isoamyl alcohol (24:1), and mixed well, followed by centrifugation (13,000 g, 15 min, 4 °C). Finally, the upper phase was transferred to a new tube and the DNA was precipitated by the addition of 0.7 volumes of isopropanol and centrifugation (16,000 g, 15 min, 4 °C). The pellet was washed with 900 µl 70% ethanol and centrifuged again for 5 min at 16,000 g and 4 °C. The supernatant was completely removed, and the pellet was dried at 60 °C for 10 min. Finally, the pellet was resuspended in 30 µl ddH_2O. The quality and quantity of the obtained gDNA used as a template for PCR were analyzed via Nanodrop One^C Spectrophotometer (Thermo Fisher Scientific, Waltham, MA, USA).

Transformation of the replicative plasmids pCnSH_R, pMixSH_R, p*Cn*SH$^{HoxEF\text{-}fusion}$_R, p*Cn*SH$^{\Delta NTD\text{-}HoxF}$+HoxE _R, p*Cn*SH+HoxE_R, pCh-HoxEF$_{Syn}$+U$_{Cn}$_R and pCh-HoxU^{swapCTD}_R into *Syn*_Δhox (i.e. a hox deletion strain carrying an chloramphenicol resistance cassette integrated into the genome at the intergenic region between slr1597 and sll1514)[14] for generation of the mutant strains *Syn*_p*Cn*SH, *Syn*_pMixSH, *Syn*_p*Cn*SH$^{HoxEF\text{-}fusion}$, *Syn*_p*Cn*SH$^{\Delta NTD\text{-}HoxF}$+HoxE, *Syn*_p*Cn*SH+HoxE, *Syn*_pCh-HoxEF$_{Syn}$+U$_{Cn}$ and *Syn*_pCh-HoxU^{swapCTD}, respectively, was performed via electroporation essentially as described previously,[74] but with slight modifications. Briefly, *Syn*_Δhox was cultivated at 30°C, 50 µmol photons m^{-2} s^{-1}, ambient (0.04%) CO_2 and 150 rpm for approximately 3 days until logarithmic growth (i.e. to an OD_{750} of 0.5-0.65). Cells from 45 ml liquid culture (or corresponding lower amounts) were harvested and the pellet was washed three times with 15 ml ice-cold HEPES (1 mM, pH 7.5). Finally, the cell pellet was resuspended in 1.5 ml HEPES solution and prepared as 60-80 µl aliquots. For transformation, 200-1000 µg of plasmid DNA were added to each aliquot of electrocompetent cells and introduced via electroporation applying 2.5 kV for 5 ms (12.5 kV cm−1) in an Eporator 4309 (Eppendorf). Immediately following the electric pulse, the cells were resuspended in 700 µL yBG11 medium and plated on BG11 agar plates containing the selective antibiotics at 50% of the normal operating concentrations (i.e. 20 µg/ml

spectinomycin). The plates were incubated at 30 °C and 25 µmol photons m^{-2} s^{-1} for approximately 4 days and then transferred to 50 µmol photons m^{-2} s^{-1}. Colonies appeared within 7-20 days. For candidate screening via test-PCR, crude cell extracts were prepared from the transformants as follows: cyanobacterial cells grown on plates were resuspended in 30 µl water and approximately 10µl 0.09-0.15 mm glass beads were added. After vortexing three times for one minute each, the suspension was incubated at 95 °C for 5 min. Subsequently, the samples were vortexed again as described before and centrifuged at 11,000 xg for 1 min. The supernatant was transferred to a new Eppendorf tube and used as a template for PCR. Mutant strains were verified via test-PCR using One Taq polymerase (New England Biolabs) and the primers PnrsB_for and HoxY-rev_2. The obtained products were different in size, depending on the chimeric hydrogenases, i.e. 3139 bp (*Cn*Hox), 4261 bp (MixSH), 3656 bp (*Cn*$SH^{HoxEF\text{-}fusion}$), 3578 bp (*Cn*$SH^{\Delta NTD\text{-}HoxF}$+HoxE), 3725 bp (*Cn*SH+HoxE), 4249 bp (Ch-$HoxEF_{Syn}$+U_{Cn}), 4242 bp (Ch-$HoxU^{swapCTD}$).

4.4. Production of chimeric hydrogenases in C. necator. Chimeric hydrogenases were produced as previously described for *Cn*SH and *Syn*HoxEFU.[9,47,50] Briefly, precultures were grown at 37°C in FN minimal medium for 24-48 h. Main cultures were grown at 30°C in FGN medium for 7 to 10 days at 130 rpm in 80% filled, baffled shaking flasks until they reached an optical density (OD_{436nm}) of 10-12. Cell pellets were harvested by centrifugation at 6000 xg for 30 min at 4°C and were frozen in liquid N_2.

4.4.1. Preparation of soluble extract. To obtain the soluble cell extract, previously produced cell pellets were thawed on ice and resuspended in a double volume of argon-saturated cell disruption buffer (50 mM Tris-HCl pH 8.0, 150 mM KCl, 5% glycerol, 5 mM NAD^+, and cOmplete™ EDTA-free protease inhibitor cocktail (Roche, Germany)). Cell disruption was performed by passaging three times through a chilled French pressure cell (G. Heinemann) at 18,000 psi. The cell lysate was centrifuged at 36,000 rpm, 1h, 4°C (Beckman Coulter Optima XE-90 ultracentrifuge) and the supernatant was immediately used for performing the activity measurements or alternatively for protein purification.

4.4.2 Protein purification. For hydrogenase purification, the soluble extract was applied to a StrepTactin™ Superflow column (iba, Göttingen, Germany) pre-equilibrated with purification buffer (50 mM Tris-HCl pH 8.0, 150 mM KCl, 5% glycerol). To remove unbound proteins, the column was sequentially washed with Wash Buffer I (50 mM Tris-HCl pH 8.0, 150 mM KCl, 5% glycerol, 5 mM NAD+) and Wash Buffer II (50 mM Tris-HCl pH 8.0, 150 mM KCl, 5% glycerol). The purified enzyme was eluted with elution buffer (50 mM Tris-HCl pH 8.0, 150 mM KCl, 5% glycerol, 5 mM desthiobiotin) and concentrated using Amicon™ Ultra-15 centrifugal filters with the appropriate molecular weight cut-off at 4000xg and 4°C. Protein concentration was determined by the BCA protein assay using bovine serum albumin as the standard (Pierce, Waltham, MA, USA). Protein production and purity was assessed by SDS-PAGE using BioRad MINI-PROTEAN™ TGX Stain-Free™ gels in TPE buffer (90 mM Tris, 10 mM EDTA, 2% (w/v) H3PO4, pH 7.6). *Synechocystis* PFOR (Sll0741) and ferredoxin 1 (Ssl0020) were purified according to the methods described by Wang et al. 2022 and Artz et al. 2020, respectively.[25,75]

4.5. Electron paramagnetic resonance (EPR) measurements. EPR samples were prepared in a 200 mM Tris-HCl buffer (pH 8.0) containing 150 mM KCl and 5% (w/v) glycerol. Aliquots of the protein solution (0.15-0.2 mM, 100 µL) were reduced anaerobically under 100% N_2 using a 50-fold excess of NADH, NADH plus 10% H_2 or sodium dithionite (DT). The EPR spectra were recorded on a Bruker EMX plus X-Band spectrometer with an ER 4122 super-high Q (SHQE) resonator and an Oxford ESR900 helium flow cryostat, with temperature control via an Oxford ITC4 controller. Baseline correction was performed by subtracting a reference spectrum of the

buffer solution recorded under the same conditions, with broad baseline drifts adjusted using a polynomial or spline function. The experimental settings were: 1 mW microwave power, 9.29 GHz microwave frequency, 10 G modulation amplitude, and 100 kHz modulation frequency.

4.6. Hydrogenase activity measurements in soluble extract. Photometric measurements were performed using an UV/Vis spectrophotometer (Varian Cary50 or Varian Cary60) to determine the H_2-mediated NAD^+-reductase activity, as previously described.[67] All measurements were performed under anaerobic conditions in H_2-saturated assay buffer (50 mM Tris-HCl, pH 8.0) in a rubber septum sealed 3 mL cuvette at 30°C. Immediately before starting the measurements, 1 mM NAD^+ was added to the reaction mixture. Optionally, 0.5 mM $NiCl_2$ and/or 5 mM $MgCl_2$ were added. The reaction was started by adding 50 µL of the respective soluble extract, which contained an average of 30 mg/mL of total protein, and the increase in absorbance at 365 nm (ε=3.3 mM^{-1} cm^{-1}) was monitored. For negative controls, measurements were performed without H_2, and with soluble cell extracts containing either the hydrogenase module only or the reductase module only. All measurements were performed with two biological replicates that were measured at least twice. Enzymatic activities were calculated as apparent specific activities where 1 mU mg^{-1} is defined as the production of 1 nmol NADH per minute per mg soluble cell extract protein under the given assay conditions.

4.7. Oxidoreductase activity measurements of purified enzymes. The ferredoxin-dependent NAD^+ reduction activity was assessed using the assay developed by Lettau et al.[9] In brief, pyruvate ferredoxin reductase (PFOR) was used as a recycling system for reduced ferredoxin. 4.5 mM ferredoxin was reduced for 30 min at room temperature (25°C) in a 1 mL reaction mixture containing 100 mM Tris-HCl buffer pH 8.0, 270 µM PFOR, 0.5 mM coenzyme A, 10 mM pyruvate, 5 mM thiamine pyrophosphate, 40 mM glucose, 40 U glucose oxidase and 50 U catalase to establish anaerobic conditions. The reaction was initiated by the addition of 1 mM NAD^+ and 65 µM of the respective enzyme, and the increase in absorbance at 340 nm (ε = 6.22 mM^{-1} cm^{-1}) was monitored spectrophotometrically. All samples were assayed in technical triplicate. NAD^+-reducing activities were given as specific activities, where 1 mU mg^{-1} corresponds to the conversion of 1 nmol NAD^+ to NADH per minute per 1 mg purified protein under the specified assay conditions.

4.8. Chemolithoautotrophic growth experiments. For autotrophic growth of *C. necator* based on chimeric hydrogenases, cultures were grown in FN minimal medium at 30°C for 48h. Cultures were then harvested and washed three times with sterile H16 buffer to remove all organic carbon sources. Cell pellets resuspended in H16 buffer were spread on AutN agar plates and incubated in an atmosphere containing 10% H_2, 10% CO_2, 5% O_2 and 75% N_2 at 30°C. Cell growth was visually monitored by colony formation for 5 to 21 days. The atmosphere was renewed periodically to ensure an adequate supply of H_2.[64] Colony PCR was performed to exclude the formation of revertants. The OneTaq MasterMix (New England BioLabs Inc.) was used for this purpose. Primer pair T114/T116 was used to verify the deletion of the reductase operon in strain HF903. Primers T104 and T111 were used to check the integrity of the corresponding plasmid. Primer pairs T117/T118 and T119/T120 were used to verify the presence of the *Cn*HoxFU genes in the genome. The size of the PCR products was checked by agarose gel electrophoresis. In addition, the PCR products were sequenced to identify mutations (MicroSynth AG).

4.9. Preparation of protein extracts from Synechocystis and Western blot analysis. For preparation of protein extracts from *Synechocystis* strains bearing genomic integration of

chimeric hydrogenases (i.e. *Syn*_HoxYH$_{Cn}$, *Syn*_MixSH, and *Syn_Cn*SH$^{HoxEF\text{-}fusion}$), 40 ml liquid cultures were grown to an OD_{750} of 3-4 as described above and harvested by centrifugation. The cell pellets were resuspended in 250 µl 50 mM potassium phosphate buffer (pH 7.0) containing 5% glycerol and 1 mM PMSF and supplemented with a glass bead mixture of three different sizes, i.e. 0.09–0.15 mm, 0.17–0.18 mm and 0.5 mm (Sartorius™, Göttingen, Germany).[67] Protein extracts were prepared using a Precellys® Evolution Super Homogenizer equipped with a Cryolys® cooling system (Bertin, France) for 3 × 30 s at 6,800 x g and 4 °C as described by Lupacchini *et al*, 2021.[30] The protein concentration of the cell extracts was determined by Bradford assay.[76] For Western blot analysis, 40 µg protein extract were separated by SDS-PAGE on 12% polyacrylamide gels and either Coomassie-stained (loading control) or transferred to a 0.2 or 0.45 µm pore size nitrocellulose membrane (GVS, Italy) via electro-blotting at 0.8 mAmp per cm^2 gel for 30 min. The membranes were blocked with 5% BSA in TBS-T for 1 h at room temperature and subsequently treated with α-*Syn*HoxE, α-*Syn*HoxF and α-*Cn*HoxH polyclonal primary antibodies diluted 1:15,000 in the blocking buffer at 4°C overnight. After washing 3 times for 10 min in TBS-T, the membranes were hybridized with horseradish peroxidase conjugated Goat α-rabbit IgG antibody (Invitrogen) diluted 1:500 in TBS-T and containing 3% BSA for 1 h at room temperature. After washing 3 times for 10 min in TBS-T, the blots were developed using WesternBright ECL Spray (Advansta, CA, USA) and analyzed in a Vilber Lourmat chemiluminescence imaging system (Vilber, France), according to manufacturer's instructions. The specific primary antibodies α-*Syn*HoxE, α-*Syn*HoxF and α-*Cn*HoxH were obtained from Eurogentec (Köln, Germany) and generated in rabbits.

For Western Blot Analysis of chimeric *Synechocystis* strains bearing chimeric hydrogenases on a replicative plasmid (i.e. *Syn*_p*Cn*SH, *Syn*_pMixSH, *Syn*_p*Cn*SH$^{HoxEF\text{-}fusion}$, Syn_pCh- 25, *Syn*_p*Cn*SH+HoxE, *Syn*_pCh-HoxEF$_{Syn}$+U$_{Cn}$ and *Syn*_pCh-HoxU^{swapCTD}), proteins were crudely extracted as follows: 200 ml culture were inoculated to an OD_{750} of 0.05 and grown in bubble columns (Kniese, Germany) to an OD_{750} of 1.0-1.5. Subsequently, they were induced with 2.5 µM or 10 µM Ni^{2+} for 24h or grown without induction. After harvesting, the cells were resuspended in extraction buffer (i.e. 50 mM KPi buffer (pH 7.0) containing 5% glycerol and 1 mM PMSF) and disrupted with glass beads of 0.17-0.19 mm in size by vortexing in a Vortex-Genie Pulse equipped with a RurboMix attachment (Scientific industries, PA, USA) for 3 min at full speed (i.e. 27,400 rpm) and 4°C. Afterwards, the beads and cell debris were pelleted by centrifuged (15 min, 20,000 x g, 4°C). The supernatant containing soluble proteins was transferred to a new tube and the protein concentration was determined by Bradford assay.[76] For Western blot analysis, 10 µg protein extract were separated by SDS-PAGE on 15% Bis-Tris polyacrylamide gels and either Coomassie-stained (loading control) or transferred to 0.45 µm pore size nitrocellulose membranes (Carl Roth GmbH + Co KG, Karlsruhe, Germany) via electro-blotting at 400 mAmp per gel for 60 min. The membranes were dried or processed immediately. Membranes for reaction with the α-*Cn*HoxH primary antibody were blocked with 5% BSA in TBS-T and reacted with the primary and secondary antibodies as described above. Membranes for reaction with α-*Syn*HoxE, and α-*Syn*HoxF antibodies were blocked with 5% milk powder in PBS for 1h at room, washed twice with PBS-T and hybridized with the polyclonal rabbit primary antibodies diluted 1:5,000 in PBS-T at 4°C overnight.[60] After washing 3 x 20 min in PBS-T, the membranes were hybridized with a horseradish peroxidase-conjugated secondary antibody (anti-rabbit, Cytiva) diluted 1:10,000 in PBS-T for 1 h at room temperature. Finally, the blot was washed 3 x 10 min in PBS-T and 2 x 10 min in PBS and exposed to Western BLoT Ultra-Sensitive HRP Substrate (Takara, CA, USA) to detect chemiluminescence using an Azure 400 Visible Fluorescent Western System (Biozym Scientific GmbH, Germany / Azure Biosystems, CA, USA), according to manufacturer's instructions.

For additional analysis of *Syn*_p*Cn*SH$^{HoxEF\text{-}fusion}$ and controls, corresponding cultures were grown, proteins were extracted and analyzed by immunoblotting as described for

Synechocystis strains bearing genomic integrated hydrogenases, but with slight modifications. If not specified otherwise, 15 µg protein extracts were applied and immunoblot analyses were performed using specific primary antibodies diluted 1:20,000 (*Cn*HoxH) or 1:10,000 (*Syn*HoxF and *Syn*HoxE) and horseradish peroxidase-conjugated secondary antibodies diluted 1:5,000.

4.11. H_2 consumption measurement in Synechocystis via gas chromatography (GC). H_2 consumption measurement via GC were performed essentially as described by Lupacchini et al.[30] For analysis of strains bearing genomic integrated hydrogenases (i.e. *Syn*_HoxYH$_{Cn}$, *Syn*_MixSH, and *Syn_Cn*SH$^{HoxEF\text{-}fusion}$), cultures were grown photoautotrophically as specified above, but with 2% CO_2 until an OD_{750} of approximately 3-4 was reached. For each GC sample, 5 ml liquid culture were transferred into a 10 ml glass vial (10 ml Crimp Top HS Vial, Thermo Scientific™) and, if appropriate, supplemented with 20 µM DCMU. The vials were sealed with gas-tight caps (C4020-42AP 20mm Magnetic Crimp Cap, 8 mm hole; Thermo Scientific™) and flushed with a gas mixture of 20% H_2, 10% CO_2, and 70% N_2 for 1 min using a gas flow mixing station (PCU-10 Display and Control Device, Vögtlin). The vials were incubated at 50 µmol photons m^{-2} s^{-1} and 150 rmp at 30°C for 72 h and measured immediately after flushing (time point 0 h) as well as after 6, 18, 24, 48 and 72 h of incubation. Specific H_2 consumption rates given in U/g_{CDW} (whereby 1 U is defined as the consumption of 1 µmol H_2 min^{-1}) were calculated based on concentration changes in the respective time periods. GC-Analysis of strains bearing chimeric hydrogenase on a replicative plasmid was performed essentially the same as for strains bearing genomic integrated hydrogenases, but cultures were pre-grown at 2% CO_2 , induced with 2.5 µM Ni^{2+} for 24h, and 5 ml aliquots were analyzed in 20 ml sealed glass vials 0, 2, 4, 6 and 8h after flushing for 1 min with a 20% H_2, 10% CO_2 and 70% N_2 gas mixture, using the above mentioned gas mixing station. GC analysis was conducted on a TRACE 1310 gas chromatograph (Thermo Scientific) equipped with a TG-Bond MIsieve column (length: 30 m; inside diameter: 0.32 mm; film thickness: 0.30 µm, Thermo Scientific). 100 µl sample were injected via automated injection using a TriPlus™ RSH SMART Autosampler (Thermo Scientific™). Measurements were performed at temperatures of the Thermal conductivity detector and oven of 100°C and 50°C, respectively. Argon was used as a carrier gas at a flow rate of 2 ml min^{-1}. The total run time was 2.4 min. H_2 and O_2 were quantified based on calibration curves obtained from measurement of defined gas mixtures (Air Products, PA, USA). The specific hydrogenase activity was calculated in units per g cell dry weight (U / g_{CDW}), whereby 1 U corresponds to consumption of 1 µmol H_2 min^{-1}. The CDW was calculated from OD_{750} using a conversion factor of 0.2246.[77] Data were normalized by subtraction of the mean H_2 loss in cell-free controls (i.e. yBG11). Analysis was performed in biological triplicates.

4.12. H_2 production measurements of purified enzymes via gas chromatography (GC). NADH-driven H_2 production by purified SH variants was quantified by gas chromatography (GC-2014AT, Shimadzu) under anaerobic conditions. Reactions were performed in 0.5 mL Tris/HCl buffer (50 mM, pH 30°C 8.0) in an 8 mL reaction vessel, both purged with nitrogen to remove other gases. NADH was added to a final concentration of 1 mM and the reaction was initiated by the addition of 1 µM purified SH. The assay was performed at 30°C with vigorous shaking for 30 minutes. Samples of 250 µL of headspace gas were collected every 5 minutes and injected into a GC Hayesep N column with a 13 × molecular sieve column and argon as the carrier gas for detection of small gases to measure hydrogen concentration. The activity was determined by calculating the µmoles of H_2 produced per minute, normalized to the enzyme mass used. 1 unit of enzyme activity (U) was defined as the production of 1 µmol H_2

per minute per milligram of protein, based on calibration and linear regression analyses of the GC data.

4.13. In vivo H_2 production measurements in Synechocystis

4.13.1. Clark-type electrode. H_2 production measurements using a Clark-type electrode and sodium dithionite (DT) reduced methyl viologen (MV) as an artificial electron donor were performed as described previously.[6] For expression of *hox* genes under the control of P_{psbA2} (i.e. *Synechocystis* strains bearing genomic integration of chimeric hydrogenase), the liquid cultures were supplemented with 17 µM ferric ammonium citrate and 1 µM $NiCl_2$ and grown photoautotrophically as described above. For expression of *hox* genes under the control of P_{nrsB}, the expression was induced with 2.5 µM Ni^{2+} for 24 h. 20 ml cultures were harvested at an OD_{750} of approximately 1.5-3.0 by centrifugation (8,228 x g, 5 min, RT) and resuspended in 300-1000 µL of the remaining supernatant or BG110 medium (i.e. BG11 medium containing sodium chloride instead of sodium nitrate) to achieve concentration for final analysis. For H_2 production measurements, culture aliquots were mixed with 5 mM MV and 10 mM DT and analysis was performed at -0.6 V at 30 °C using a Clark-type electrode connected to an Oxy/Eco Current box (Hansatech) and recorded applying OxyTrace+ software for 5 to 15 min. The specific hydrogenase activity was calculated from the signal slope in the range of linear H_2 increase and is given in units per g cell dry weight (U/g_{CDW}), whereby 1 U corresponds to production of 1 µmol H_2 min^{-1}. The CDW was calculated from OD_{750} using a conversion factor of 0.2246.[77] Data were normalized by subtraction of the H_2 turnover of the corresponding reference strain (*Syn*_Δhox' or *Syn*_Δhox, respectively). Analysis was performed in 2-6 biological replicates as specified in the figure legends.

4.13.2. Unisense hydrogen electrode. H_2 production measurements in *Synechocystis* under fermentative and photosynthetic conditions using a microsensor H_2-50 (Unisense, Aarhus, Denmark) were performed as described previously.[78] Liquid cultures supplemented with 17 µM ferric ammonium citrate and 1 µM $NiCl_2$ were grown photoautotrophically to an OD_{750} of approximately 1.5-3.0. Cells from 20 ml liquid culture were harvested by centrifugation (8,228 x g, 5 min, RT) and resuspended in 1 ml BG110 medium (BG11 medium containing sodium chloride instead of sodium nitrate). The chlorophyll content was determined[79] and cell suspensions containing 20 µg ml^{-1} chlorophyll were placed in a cuvette of the Dual-KLAS/NIR (Walz, Germany). The samples were adjusted to a final volume of 1.6 ml, and supplemented with glucose, glucose oxidase and catalase to final concentrations of 10 mM, 40 U / ml and 50 U / ml, respectively. A hydrogen electrode placed in a lab-made holder[78] was inserted and fermentative H_2 turnovers were measured in the dark for 5-20 h (until a maximum in H_2 production was exceeded). Subsequently, a light with 750 µE / m^2 / s was switched on and the hydrogen turnover under photosynthetic conditions was measured for another 30-200 min. Data are presented as µmol H_2 produced / L or as maximal H_2 production activities given in µM / min / g_{CDW}. The later was calculated from the maximum slope of biological duplicates under the respective condition and normalized by subtraction of the H_2 turnover of the reference strain *Syn*_Δhox'. The CDW was calculated from OD_{750} using a conversion factor of 0.2246.[77]

4.13.3. GC measurements. For H_2 production under photosynthetic conditions, *Synechocystis* cultures were cultivated up to an OD_{750} of 2.5-3, centrifuged (4000 g, 5 min and RT) and resuspended in 0.1 M KP_i buffer (pH 7.2) to a final OD_{750} of 2.5. Aliquots (5 ml) of *Synechocystis* cultures, with optional supplementation of 10 mM glucose, were incubated in 20 ml sealed glass vials. The headspace of all vials was flushed for 2 minutes with N_2 to create anoxic conditions and vials were incubated at 30°C, 150 rpm, 200 $\mu mol \cdot m^{-2} \cdot s^{-1}$.). Gas composition was determined regularly via GC for up to 144 hours. H_2 and O_2 were quantified

using calibration curves of both gases, determined with defined gas mixtures (Air Products, PA, USA). The H_2ase specific activity was calculated in µmol H_2/grams of cell dry weight (CDW). The CDW was calculated from OD_{750} using a conversion factor of 0.2246.[77] Data were normalized by subtraction of the mean H_2 increase in cell-free controls (yBG11). Analysis was performed in biological triplicates.

4.14. Statistical analysis. For statistical analyses of data, the program IBM® SPSS® Statistics Version 29.0.0.0 was applied. If Levene's tests revealed no significant differences ($p > 0.05$) between the variances of specific H_2 production and consumption activities of cyanobacterial strains, ANOVA ($p < 0.05$) followed by post-hoc Tukey multiple comparison tests was performed. If Levene's tests revealed significant differences ($p < 0.05$) between the variances, Welch-ANOVA ($p < 0.05$) followed by post-hoc Games-Howell multiple comparison tests was performed. For comparison of 2 samples (i.e. induced versus uninduced strains bearing chimeric hydrogenases on a replicative plasmid), 2 sample t-tests ($p < 0.05$) were performed. Results are provided in in the supplementary information 2 (Statistics S1-S3).

4.15. Computational methods. Protein structure models for CnSH and SynSH were generated using the AlphaFold 3.0 algorithm and evaluated using the per-residue confidence score (pLDDT) and overall structure reliability metrics.[36,37,39] Structural accuracy was further assessed using the predicted template modelling score (pTM) and the interface predicted modelling score (ipTM) to validate the reliability of subunit positioning and overall model quality. To obtain holoenzyme models, the AlphaFill algorithm was used to incorporate ligands, cofactors and metal centers into the predicted structures.[38]

Abbreviations. aa – amino acid, *C. necator* – *Curiavidus necator* H16, CTD – C-terminal domain, DCMU - 3-(3,4-dichlorophenyl)-1,1-dimethylurea, DT – sodium dithionite, EPR – electron paramagnetic resonance, Fd – ferredoxin, FNR – ferredoxin-NADPH reductase, Hox(E)FU – SH reductase module, HoxYH – SH hydrogenase module, MBH – membrane bound hydrogenase, MV – methyl viologen, NAD(P)+/H - nicotinamide adenine dinucleotide phosphate, NTD – N-terminal domain, PET – photosynthetic electron transport, PetF – ferredoxin 1, PS I – photosystem I, PS II – photosystem II, PQ – plastoquinone, RC I – respiratory complex I, SH – soluble NAD^+-reducing hydrogenase, *Synechocystis* – *Synechocystis* sp. PCC 6803

Supporting Information. Supplementary Information 1 contains additional details on enzyme and strain characterization, supporting figures and tables (PDF), Supplementary Information 2 contains all statistical information (PDF), Supplementary Information 3 contains all plasmid sequences (DOC).

Data availability. The authors confirm that the data supporting the findings of this study are available within the article and/or its supplementary materials. Data on the design of chimeric hydrogenases in *C. necator*, as well as on their biochemical examination, are available in [repository name] at [URL], reference number [reference number].

Author Information. E.L. and L.L. - RWTH Aachen University, iAMB – Institute of Applied Microbiology, Worringer Weg 1, 52074 Aachen (Germany); E.L. and C.L. - Technische Universität Berlin, Institute for Chemistry, Straße des 17. Juni 135, 10623 Berlin (Germany); Ja.T., Jö.T, D.S. and B.B. - Helmholtz Centre for Environmental Research – UFZ-Leipzig, Department of Microbial Biotechnology, Permoserstraße 15, 04318 Leipzig, (Germany); Ja.T., R.M. and A.M-A. - TU Wien, Institute of Chemical, Environmental and Bioscience Engineering – ICEBE, Gumpendorfer Straße 1a, 1060 Wien (Austria); J.A., M.B. and K.G. - Universität Kassel, Institut für Biologie, Heinrich-Plett-Straße 40, 34132 Kassel (Germany); C.T. - Freie Universität Berlin, Institute für Physik, Arnimallee 14, 14195 Berlin (Germany)

Author Contribution. E.L.: conceptualization, investigation, methodology, validation, visualization, writing – original draft, editing and review. Ja.T.: funding acquisition, conceptualization, investigation, methodology, validation, visualization and writing – original draft. J.A.: methodology, validation, visualization. M.B.: methodology. K.G.: funding acquisition, project administration. Jö.T.: project administration, supervision. D.S.: investigation, methodology, validation, writing—review and editing. C.L. investigation, methodology, validation. C.T.: investigation, methodology, validation. R.M.: supervision. A.M-A.: supervision. B.B. conceptualization, funding acquisition, project

administration, supervision, and writing—review and editing. L.L.: conceptualization, funding acquisition, project administration, supervision, and writing—review and editing.

Conflict of Interest. The authors declare no conflict of interest.

Acknowledgment. The authors received the support of the German Research Foundation (E.L. and L.L - DFG grant no. 405325648, 550624628 and C. L. - SPP 1927 within DFG grant no. 311062227 (ZE 510/2-2)) and the Austrian Science Fund (FWF grant J4485-B, Ja.T.). L.L. acknowledge the financial support from the Deutsche Forschungsgemeinschaft (DFG) under Germany's Excellence Strategy: The Fuel Science Center (EXC 2186 390919832) and by the Werner Siemens Foundation (WSS) through the Forschungszentrum catalaix. We thank Oliver Lenz (Technische Universität Berlin) for his generous support and helpful discussions as well as for providing lab space and equipment. Moreover, we thank Astrid R. Mach-Aigner for providing supervision, equipment and lab space at the TU Wien. Honourable mentions to Rafał Piwowarczyk and Frederic Radzio for their research internship contributions.

References

(1) Gutekunst, K.; Chen, X.; Schreiber, K.; Kaspar, U.; Makam, S.; Appel, J. The Bidirectional NiFe-Hydrogenase in *Synechocystis* sp. PCC 6803 Is Reduced by Flavodoxin and Ferredoxin and Is Essential under Mixotrophic, Nitrate-Limiting Conditions *. *J. Biol. Chem.* **2014**, *289* (4), 1930–1937.

(2) Peters, J. W.; Schut, G. J.; Boyd, E. S.; Mulder, D. W.; Shepard, E. M.; Broderick, J. B.; King, P. W.; Adams, M. W. W. [FeFe]- and [NiFe]-Hydrogenase Diversity, Mechanism, and Maturation. *BBA - Mol. Cell Res.* **2015**, *1853* (6), 1350–1369.

(3) Yacoby, I.; Pochekailov, S.; Toporik, H.; Ghirardi, M. L.; King, P. W.; Zhang, S. Photosynthetic Electron Partitioning between [FeFe]-Hydrogenase and Ferredoxin:NADP$^+$-Oxidoreductase (FNR) Enzymes in Vitro. *Proc. Natl. Acad. Sci.* **2011**, *108* (23), 9396–9401.

(4) McIntosh, C. L.; Germer, F.; Schulz, R.; Appel, J.; Jones, A. K. The [NiFe]-Hydrogenase of the Cyanobacterium *Synechocystis* sp. PCC 6803 works Bidirectionally with a Bias to H_2 Production. *JACS.* **2011**, *133* (29), 11308–11319.

(5) Finkelmann, A. R.; Stiebritz, M. T.; Reiher, M. Activation Barriers of Oxygen Transformation at the Active Site of [FeFe] Hydrogenases. *Inorg. Chem.* **2014**, *53* (22), 11890–11902.

(6) Gutthann, F.; Egert, M.; Marques, A.; Appel, J. Inhibition of Respiration and Nitrate Assimilation Enhances Photohydrogen Evolution under Low Oxygen Concentrations in *Synechocystis* sp. PCC 6803. *BBA - Bioenerg.* **2007**, *1767* (2), 161–169.

(7) Cournac, L.; Guedeney, G.; Peltier, G.; Vignais, P. M. Sustained Photoevolution of Molecular Hydrogen in a Mutant of *Synechocystis* sp. Strain PCC 6803 Deficient in the Type I NADPH-Dehydrogenase Complex. *J. Bacteriol.* **2004**, *186* (6), 1737–1746.

(8) Sun, Y.; Chen, M.; Yang, H.; Zhang, J.; Kuang, T.; Huang, F. Enhanced H_2 Photoproduction by Down-Regulation of Ferredoxin-NADP+ Reductase (FNR) in the Green Alga *Chlamydomonas Reinhardtii*. *Int. J. Hydrog. Energy* **2013**, *38* (36), 16029–16037.

(9) Lettau, E.; Lorent, C.; Appel, J.; Boehm, M.; Cordero, P. R. F.; Lauterbach, L. Insights into Electron Transfer and Bifurcation of the *Synechocystis* sp. PCC6803 Hydrogenase Reductase Module. *BBA - Bioenerg.* **2025**, *1866* (1), 149508.

(10) Eilenberg, H.; Weiner, I.; Ben-Zvi, O.; Pundak, C.; Marmari, A.; Liran, O.; Wecker, M. S.; Milrad, Y.; Yacoby, I. The Dual Effect of a Ferredoxin-Hydrogenase Fusion Protein in Vivo: Successful Divergence of the Photosynthetic Electron Flux towards Hydrogen Production and Elevated Oxygen Tolerance. *Biotechnol. Biofuels* **2016**, *9* (1), 182.

(11) Weiner, I.; Shahar, N.; Feldman, Y.; Landman, S.; Milrad, Y.; Ben-Zvi, O.; Avitan, M.; Dafni, E.; Schweitzer, S.; Eilenberg, H.; Atar, S.; Diament, A.; Tuller, T.; Yacoby, I. Overcoming the Expression Barrier of the Ferredoxin-hydrogenase Chimera in *Chlamydomonas reinhardtii* Supports a Linear Increment in Photosynthetic Hydrogen Output. *Algal Res.* **2018**, *33*, 310–315.

(12) Ihara, M.; Nishihara, H.; Yoon, K.-S.; Lenz, O.; Friedrich, B.; Nakamoto, H.; Kojima, K.; Honma, D.; Kamachi, T.; Okura, I. Light-Driven Hydrogen Production by a Hybrid Complex of a [NiFe]-Hydrogenase and the Cyanobacterial Photosystem I. *Photochem. Photobiol.* **2006**, *82* (3), 676–682.

(13) Schwarze, A.; Kopczak, M. J.; Rögner, M.; Lenz, O. Requirements for Construction of a Functional Hybrid Complex of Photosystem I and [NiFe]-Hydrogenase. *Appl. Environ. Microbiol.* **2010**, *76* (8), 2641–2651.

(14) Appel, J.; Hueren, V.; Boehm, M.; Gutekunst, K. Cyanobacterial in Vivo Solar Hydrogen Production Using a Photosystem I–Hydrogenase (PsaD-HoxYH) Fusion Complex. *Nat. Energy* **2020**, *5* (6), 458–467.

(15) Kanygin, A.; Milrad, Y.; Thummala, C.; Reifschneider, K.; Baker, P.; Marco, P.; Yacoby, I.; E. Redding, K. Rewiring Photosynthesis: A Photosystem I-Hydrogenase Chimera That Makes H_2 in Vivo. *Energy Environ. Sci.* **2020**, *13* (9), 2903–2914.

(16) Burgdorf, T.; Lenz, O.; Buhrke, T.; van der Linden, E.; Jones, A. K.; Albracht, S. P. J.; Friedrich, B. [NiFe]-Hydrogenases of *Ralstonia eutropha* H16: Modular Enzymes for Oxygen-Tolerant Biological Hydrogen Oxidation. *J. Mol. Microbiol. Biotechnol.* **2006**, *10* (2–4), 181–196.
(17) Lauterbach, L.; Lenz, O. Catalytic Production of Hydrogen Peroxide and Water by Oxygen-Tolerant [NiFe]-Hydrogenase during H_2 Cycling in the Presence of O_2. *JACS.* **2013**, *135* (47), 17897–17905.
(18) Schneider, K.; Schlegel, H. G. Purification and Properties of Soluble Hydrogenase from *Alcaligenes eutrophus* H16. *BBA - Enzymol.* **1976**, *452* (1), 66–80.
(19) Horch, M.; Lauterbach, L.; Lenz, O.; Hildebrandt, P.; Zebger, I. NAD(H)-Coupled Hydrogen Cycling – Structure–Function Relationships of Bidirectional [NiFe] Hydrogenases. *FEBS Lett.* **2012**, *586* (5), 545–556.
(20) Burgdorf, T.; van der Linden, E.; Bernhard, M.; Yin, Q. Y.; Back, J. W.; Hartog, A. F.; Muijsers, A. O.; de Koster, C. G.; Albracht, S. P. J.; Friedrich, B. The Soluble NAD^+-Reducing [NiFe]-Hydrogenase from *Ralstonia eutropha* H16 Consists of Six Subunits and Can Be Specifically Activated by NADPH. *J. Bacteriol.* **2005**, *187* (9), 3122–3132.
(21) Grzeszik, C.; Lübbers, M.; Reh, M.; Schlegel, H. G. Genes Encoding the NAD^+-Reducing Hydrogenase of *Rhodococcus opacus* MR11. *Microbiology* **1997**, *143* (4), 1271–1286.
(22) Suzuki, S.; Kuenen, J. G.; Schipper, K.; van der Velde, S.; Ishii, S.; Wu, A.; Sorokin, D. Y.; Tenney, A.; Meng, X.; Morrill, P. L.; Kamagata, Y.; Muyzer, G.; Nealson, K. H. Physiological and Genomic Features of Highly Alkaliphilic Hydrogen-Utilizing Betaproteobacteria from a Continental Serpentinizing Site. *Nat. Commun.* **2014**, *5* (1), 3900.
(23) Schmitz, O.; Boison, G.; Salzmann, H.; Bothe, H.; Schütz, K.; Wang, S.; Happe, T. HoxE—a Subunit Specific for the Pentameric Bidirectional Hydrogenase Complex (HoxEFUYH) of Cyanobacteria. *BBA - Bioenerg.* **2002**, *1554* (1), 66–74.
(24) Preissler, J.; Reeve, H. A.; Zhu, T.; Nicholson, J.; Urata, K.; Lauterbach, L.; Wong, L. L.; Vincent, K. A.; Lenz, O. Dihydrogen-Driven NADPH Recycling in Imine Reduction and P450-Catalyzed Oxidations Mediated by an Engineered O_2-Tolerant Hydrogenase. *ChemCatChem* **2020**, *12* (19), 4853–4861.
(25) Artz, J. H.; Tokmina-Lukaszewska, M.; Mulder, D. W.; Lubner, C. E.; Gutekunst, K.; Appel, J.; Bothner, B.; Boehm, M.; King, P. W. The Structure and Reactivity of the HoxEFU Complex from the Cyanobacterium *Synechocystis* sp. PCC 6803. *J. Biol. Chem.* **2020**, *295* (28), 9445–9454.
(26) Aubert-Jousset, E.; Cano, M.; Guedeney, G.; Richaud, P.; Cournac, L. Role of HoxE Subunit in *Synechocystis* sp. PCC6803 Hydrogenase. *FEBS J.* **2011**, *278* (21), 4035–4043.
(27) Joern, J. M.; Meinhold, P.; Arnold, F. H. Analysis of Shuffled Gene Libraries. *J. Mol. Biol.* **2002**, *316* (3), 643–656.
(28) Preissler, J.; Wahlefeld, S.; Lorent, C.; Teutloff, C.; Horch, M.; Lauterbach, L.; Cramer, S. P.; Zebger, I.; Lenz, O. Enzymatic and Spectroscopic Properties of a Thermostable [NiFe]-hydrogenase Performing H_2-Driven NAD^+-Reduction in the Presence of O_2. *BBA - Bioenerg.* **2018**, *1859* (1), 8–18.
(29) Porthun, A.; Bernhard, M.; Friedrich, B. Expression of a Functional NAD^+-Reducing [NiFe] Hydrogenase from the Gram-Positive *Rhodococcus opacus* in the Gram-Negative *Ralstonia eutropha*. *Arch. Microbiol.* **2002**, *177* (2), 159–166.
(30) Lupacchini, S.; Appel, J.; Stauder, R.; Bolay, P.; Klähn, S.; Lettau, E.; Adrian, L.; Lauterbach, L.; Bühler, B.; Schmid, A.; Toepel, J. Rewiring Cyanobacterial Photosynthesis by the Implementation of an Oxygen-Tolerant Hydrogenase. *Metab. Eng.* **2021**, *68*, 199–209.
(31) Lupacchini, S.; Stauder, R.; Opel, F.; Klähn, S.; Schmid, A.; Bühler, B.; Toepel, J. Co-Expression of Auxiliary Genes Enhances the Activity of a Heterologous O_2-Tolerant Hydrogenase in the Cyanobacterium *Synechocystis* sp. PCC 6803. *Biotechnol. Biofuels Bioprod.* **2025**, *18* (1), 41.
(32) Erkens, A.; Schneider, K.; Müller, A. The NAD^+-Linked Soluble Hydrogenase from *Alcaligenes eutrophus* H16: Detection and Characterization of EPR Signals Deriving from Nickel and Flavin. *JBIC.* **1996**, *1* (2), 99–110.
(33) Germer, F.; Zebger, I.; Saggu, M.; Lendzian, F.; Schulz, R.; Appel, J. Overexpression, Isolation, and Spectroscopic Characterization of the Bidirectional [NiFe] Hydrogenase from *Synechocystis* sp. PCC 6803. *JBC.* **2009**, *284* (52), 36462–36472.
(34) Lauterbach, L.; Wang, H.; Horch, M.; B. Gee, L.; Yoda, Y.; Tanaka, Y.; Zebger, I.; Lenz, O.; P. Cramer, S. Nuclear Resonance Vibrational Spectroscopy Reveals the FeS Cluster Composition and Active Site Vibrational Properties of an O_2 -Tolerant NAD^+-Reducing [NiFe] Hydrogenase. *Chem. Sci.* **2015**, *6* (2), 1055–1060.
(35) Horch, M.; Lauterbach, L.; Saggu, M.; Hildebrandt, P.; Lendzian, F.; Bittl, R.; Lenz, O.; Zebger, I. Probing the Active Site of an O_2-Tolerant NAD^+-Reducing [NiFe]-Hydrogenase from *Ralstonia eutropha* H16 by In Situ EPR and FTIR Spectroscopy. *Angew. Chem. Int. Ed.* **2010**, *49* (43), 8026–8029.
(36) Jumper, J.; Evans, R.; Pritzel, A.; Green, T.; Figurnov, M.; Ronneberger, O.; Tunyasuvunakool, K.; Bates, R.; Žídek, A.; Potapenko, A.; Bridgland, A.; Meyer, C.; Kohl, S. A. A.; Ballard, A. J.; Cowie, A.; Romera-Paredes, B.; Nikolov, S.; Jain, R.; Adler, J.; Back, T.; Petersen, S.; Reiman, D.; Clancy, E.; Zielinski, M.; Steinegger, M.; Pacholska, M.; Berghammer, T.; Bodenstein, S.; Silver, D.; Vinyals, O.; Senior, A. W.; Kavukcuoglu, K.; Kohli, P.; Hassabis, D. Highly Accurate Protein Structure Prediction with AlphaFold. *Nature* **2021**, *596* (7873), 583–589.
(37) Evans, R.; O'Neill, M.; Pritzel, A.; Antropova, N.; Senior, A.; Green, T.; Žídek, A.; Bates, R.; Blackwell, S.; Yim, J.; Ronneberger, O.; Bodenstein, S.; Zielinski, M.; Bridgland, A.; Potapenko, A.; Cowie, A.; Tunyasuvunakool, K.;

Jain, R.; Clancy, E.; Kohli, P.; Jumper, J.; Hassabis, D. Protein Complex Prediction with AlphaFold-Multimer. bioRxiv March 10, 2022, p 2021.10.04.463034. https://doi.org/10.1101/2021.10.04.463034.
(38) Hekkelman, M. L.; de Vries, I.; Joosten, R. P.; Perrakis, A. AlphaFill: Enriching AlphaFold Models with Ligands and Cofactors. *Nat. Methods* **2023**, *20* (2), 205–213.
(39) Mariani, V.; Biasini, M.; Barbato, A.; Schwede, T. lDDT: A Local Superposition-Free Score for Comparing Protein Structures and Models Using Distance Difference Tests. *Bioinformatics* **2013**, *29* (21), 2722–2728.
(40) Zhang, Y.; Skolnick, J. Scoring Function for Automated Assessment of Protein Structure Template Quality. *Proteins Struct. Funct. Bioinf.* **2004**, *57* (4), 702–710.
(41) Xu, J.; Zhang, Y. How Significant Is a Protein Structure Similarity with TM-Score = 0.5? *Bioinformatics* **2010**, *26* (7), 889–895.
(42) Boison, G.; Schmitz, O.; Schmitz, B.; Bothe, H. Unusual Gene Arrangement of the Bidirectional Hydrogenase and Functional Analysis of Its Diaphorase Subunit HoxU in Respiration of the Unicellular Cyanobacterium *Anacystis nidulans*. *Curr. Microbiol.* **1998**, *36* (5), 253–258.
(43) Coldren, C. D.; Hellinga, H. W.; Caradonna, J. P. The Rational Design and Construction of a Cuboidal Iron–Sulfur Protein. *Proc. Natl. Acad. Sci.* **1997**, *94* (13), 6635–6640.
(44) Grzyb, J.; Xu, F.; Nanda, V.; Łuczkowska, R.; Reijerse, E.; Lubitz, W.; Noy, D. Empirical and Computational Design of Iron-Sulfur Cluster Proteins. *BBA - Bioenerg.* **2012**, *1817* (8), 1256–1262.
(45) Schneider, K.; Cammack, R.; Schlegel, H. G.; Hall, D. O. The Iron-Sulphur Centres of Soluble Hydrogenase from *Alcaligenes eutrophus*. *BBA - Protein Struct.* **1979**, *578* (2), 445–461.
(46) Uhlmann, M.; Friedrich, T. EPR Signals Assigned to Fe/S Cluster N1c of the *Escherichia col*i NADH:Ubiquinone Oxidoreductase (Complex I) Derive from Cluster N1a. *Biochemistry* **2005**, *44* (5), 1653–1658.
(47) van der Linden, E.; Burgdorf, T.; de Lacey, A. L.; Buhrke, T.; Scholte, M.; Fernandez, V. M.; Friedrich, B.; Albracht, S. P. J. An Improved Purification Procedure for the Soluble [NiFe]-Hydrogenase of *Ralstonia eutropha*: New Insights into Its (in)Stability and Spectroscopic Properties. *JBIC.* **2006**, *11* (2), 247–260.
(48) Jones, A. K.; Lenz, O.; Strack, A.; Buhrke, T.; Friedrich, B. NiFe Hydrogenase Active Site Biosynthesis: Identification of Hyp Protein Complexes in *Ralstonia eutropha*. *Biochemistry* **2004**, *43* (42), 13467–13477.
(49) Preissler, J. Funktion, Modifikation und Anwendung von O_2-toleranten, NAD(P)$^+$-reduzierenden [NiFe]-Hydrogenasen. Dissertation - Technische Universität Berlin **2018**. https://doi.org/10.14279/DEPOSITONCE-7446.
(50) Lauterbach, L.; Idris, Z.; Vincent, K. A.; Lenz, O. Catalytic Properties of the Isolated Diaphorase Fragment of the NAD$^+$-Reducing [NiFe]-Hydrogenase from *Ralstonia eutropha*. *PLOS ONE* **2011**, *6* (10), e25939.
(51) Tiemeyer, A.; Link, H.; Weuster-Botz, D. Kinetic Studies on Autohydrogenotrophic Growth of *Ralstonia eutropha* with Nitrate as Terminal Electron Acceptor. *Appl. Microbiol. Biotechnol.* **2007**, *76* (1), 75–81.
(52) Jahn, M.; Crang, N.; Gynnå, A. H.; Kabova, D.; Frielingsdorf, S.; Lenz, O.; Charpentier, E.; Hudson, E. P. The Energy Metabolism of *Cupriavidus necator* in Different Trophic Conditions. *Appl. Environ. Microbiol.* **2024**, *90* (10), e00748-24.
(53) Eckert, C.; Boehm, M.; Carrieri, D.; Yu, J.; Dubini, A.; Nixon, P. J.; Maness, P.-C. Genetic Analysis of the Hox Hydrogenase in the Cyanobacterium *Synechocystis* sp. PCC6803 Reveals Subunit Roles in Association, Assembly, Maturation, and Function. *JBC.* **2012**, *287* (52), 43502–43515.
(54) Schneider, K.; Schlegel, H. G.; Jochim, K. Effect of Nickel on Activity and Subunit Composition of Purified Hydrogenase from *Nocardia opaca* 1b. *Eur. J. Biochem.* **1984**, *138* (3), 533–541.
(55) Strittmatter, C. S.; Eggers, J.; Biesgen, V.; Pauels, I.; Becker, F.; Steinbüchel, A. The Reliance of Glycerol Utilization by *Cupriavidus necator* on CO_2 Fixation and Improved Glycerol Catabolism. *Appl. Microbiol. Biotechnol.* **2022**, *106* (7), 2541–2555.
(56) Blahut, M. R.; Dawson, M. E.; Kisgeropoulos, E. C.; Ledinina, A. E.; Mulder, D. W.; King, P. W. Functional Roles of the [2Fe-2S] Clusters in *Synechocystis* sp. PCC 6803 Hox [NiFe]-Hydrogenase Reactivity with Ferredoxins. *J. Biol. Chem.* **2024**, *300* (12).
(57) Romig, M.; Eberwein, M.; Deobald, D.; Schmid, A. Reactivation and Long-Term Stabilization of the [NiFe] Hox Hydrogenase of *Synechocystis* sp. PCC6803 by Glutathione after Oxygen Exposure. *JBC.* **2025**, *301* (1).
(58) Blasi, B.; Peca, L.; Vass, I.; Kós, P. B. Characterization of Stress Responses of Heavy Metal and Metalloid Inducible Promoters in *Synechocystis* sp. PCC6803. **2012**, *22* (2), 166–169.
(59) Heidorn, T.; Camsund, D.; Huang, H.-H.; Lindberg, P.; Oliveira, P.; Stensjö, K.; Lindblad, P. Chapter Twenty-Four - Synthetic Biology in Cyanobacteria: Engineering and Analyzing Novel Functions. In *Methods in Enzymology*; Voigt, C., Ed.; Synthetic Biology, Part A; Academic Press, 2011; Vol. 497, pp 539–579.
(60) Burroughs, N. J.; Boehm, M.; Eckert, C.; Mastroianni, G.; Spence, E. M.; Yu, J.; Nixon, P. J.; Appel, J.; Mullineaux, C. W.; Bryan, S. J. Solar Powered Biohydrogen Production Requires Specific Localization of the Hydrogenase. *Energy Environ. Sci.* **2014**, *7* (11), 3791–3800.
(61) Lim, H. N.; Lee, Y.; Hussein, R. Fundamental Relationship between Operon Organization and Gene Expression. *Proc. Natl. Acad. Sci.* **2011**, *108* (26), 10626–10631.
(62) Zhang, X.; Betterle, N.; Hidalgo Martinez, D.; Melis, A. Recombinant Protein Stability in Cyanobacteria. *ACS Synth. Biol.* **2021**, *10* (4), 810–825.
(63) Hanahan, D. Studies on Transformation of *Escherichia coli* with Plasmids. *J. Mol. Biol.* **1983**, *166* (4), 557–580.

(64) Alhafiz, H. A.; Di Bisceglie, F.; Meier, H. P. F.; Weickardt, I.; González, I. A. C.; Navarro, J. G.; Schoenmakers, P.; Oyen, S. J.; Lettau, E.; Lombard, E.; Cordero, P. R. F.; Konarzycka-Bessler, M.; Gorret, N.; Schmidt, S.; Schillberg, S.; Mann, M.; Guillouet, S. E.; Kratzer, R.; Lauterbach, L. *Cupriavidus necator* as a Model Organism for CO_2-Based Biotechnology. In *Methods in Enzymology*; Academic Press, 2025. https://doi.org/10.1016/bs.mie.2025.01.017.
(65) Shcolnick, S.; Shaked, Y.; Keren, N. A Role for mrgA, a DPS Family Protein, in the Internal Transport of Fe in the Cyanobacterium *Synechocystis* sp. PCC6803. *BBA - Bioenerg.* **2007**, *1767* (6), 814–819.
(66) Rippka, R.; Deruelles, J.; Waterbury, J. B.; Herdman, M.; Stanier, R. Y. Generic Assignments, Strain Histories and Properties of Pure Cultures of Cyanobacteria. *Microbiol.* **1979**, *111* (1), 1–61.
(67) Lenz, O.; Lauterbach, L.; Frielingsdorf, S. O_2-Tolerant [NiFe]-Hydrogenases of *Ralstonia eutropha* H16: Physiology, Molecular Biology, Purification, and Biochemical Analysis. In *Methods in Enzymology*; Armstrong, F., Ed.; Enzymes of Energy Technology; Academic Press, 2018; Vol. 613, pp 117–151.
(68) Marx, C. J.; Lidstrom, M. E. Development of Improved Versatile Broad-Host-Range Vectors for Use in Methylotrophs and Other Gram-Negative bacteria. *Microbiol.* **2001**, *147* (8), 2065–2075.
(69) Schwartz, E.; Gerischer, U.; Friedrich, B. Transcriptional Regulation of *Alcaligenes eutrophus* Hydrogenase Genes. *J. Bacteriol.* **1998**, *180* (12), 3197–3204.
(70) Gibson, D. G. Chapter Fifteen - Enzymatic Assembly of Overlapping DNA Fragments. In *Methods in Enzymology*; Voigt, C., Ed.; Synthetic Biology, Part B; Academic Press, 2011; Vol. 498, pp 349–361.
(71) Karstens, K. Untersuchungen zur Funktion sauerstofftoleranter, NAD^+-reduzierender Hydrogenasen und zu deren Anwendung in der lichtgetriebenen Wasserstoffproduktion in Cyanobakterien. Dissertation - Humboldt-Universität zu Berlin, **2015**. https://doi.org/10.18452/17123.
(72) Martínez-García, E.; Goñi-Moreno, A.; Bartley, B.; McLaughlin, J.; Sánchez-Sampedro, L.; del Pozo, H. P.; Hernández, C. P.; Marletta, A. S.; De Lucrezia, D.; Sánchez-Fernández, G.; Fraile, S.; de Lorenzo, V. SEVA 3.0: An Update of the Standard European Vector Architecture for Enabling Portability of Genetic Constructs among Diverse Bacterial Hosts. *Nucleic Acids Res.* **2020**, *48* (6), 3395.
(73) Wilson, K. Preparation of Genomic DNA from Bacteria. *Curr. Protoc. Mol. Biol.* **2001**, *56* (1), 2.4.1-2.4.5.
(74) Brandenburg, F.; Theodosiou, E.; Bertelmann, C.; Grund, M.; Klähn, S.; Schmid, A.; Krömer, J. O. *Trans*-4-Hydroxy-L-Proline Production by the Cyanobacterium *Synechocystis* sp. PCC 6803. *Metab. Eng. Commun.* **2021**, *12*, e00155.
(75) Wang, Y.; Chen, X.; Spengler, K.; Terberger, K.; Boehm, M.; Appel, J.; Barske, T.; Timm, S.; Battchikova, N.; Hagemann, M.; Gutekunst, K. Pyruvate:Ferredoxin Oxidoreductase and Low Abundant Ferredoxins Support Aerobic Photomixotrophic Growth in Cyanobacteria. *eLife* **2022**, *11*, e71339.
(76) Bradford, M. M. A Rapid and Sensitive Method for the Quantitation of Microgram Quantities of Protein Utilizing the Principle of Protein-Dye Binding. *Anal. Biochem.* **1976**, *72* (1), 248–254.
(77) Hoschek, A.; Toepel, J.; Hochkeppel, A.; Karande, R.; Bühler, B.; Schmid, A. Light-Dependent and Aeration-Independent Gram-Scale Hydroxylation of Cyclohexane to Cyclohexanol by CYP450 Harboring *Synechocystis* sp. PCC 6803. *Biotechnol. J.* **2019**, *14* (8), 1800724.
(78) Appel, J.; Craig, S.; Theune, M.; Hüren, V.; Künzel, S.; Forberich, B.; Bryan, S.; Gutekunst, K. Evidence for Electron Transfer from the Bidirectional Hydrogenase to the Photosynthetic Complex I (NDH-1) in the Cyanobacterium *Synechocystis* sp. PCC 6803. *Microorg.* **2022**, *10* (8), 1617.
(79) Lichtenthaler, H. K. [34] Chlorophylls and Carotenoids: Pigments of Photosynthetic Biomembranes. In *Methods in Enzymology*; Plant Cell Membranes; Academic Press, 1987; Vol. 148, pp 350–382.